

1 **Does increasing spatial resolution improve the**
2 **simulation of United Kingdom daily precipitation in a**
3 **regional climate model?**

4 **Steven C. Chan · Elizabeth J. Kendon ·**
5 **Hayley J. Fowler · Stephen Blenkinsop ·**
6 **Christopher A. T. Ferro · David B.**
7 **Stephenson**

8
9 Received: date / Accepted: date

10 **Abstract** Three different resolution (50, 12, and 1.5 km) regional climate model
11 simulations are compared in terms of their ability to simulate moderate and high
12 daily precipitation events over the southern United Kingdom. Among the three
13 simulations, the convection-permitting 1.5-km simulation is carried out without
14 convective parametrisation. As in previous studies, increasing resolution (espe-
15 cially from 50 km to 12 km) is found to improve the representation of orographic
16 precipitation. The 50-km simulation underestimates mean precipitation over the
17 mountainous region of Wales, and event intensity tends to be too weak; this bias
18 is reduced in both the 12-km and 1.5-km simulations for both summer and winter.
19 In south-east England lowlands where summer extremes are mostly convective, in-
20 creasing resolution does not necessary lead to an improvement in the simulation.
21 For the 12-km simulation, simulated daily extreme events are overly intense. Even
22 though the average intensity of summer daily extremes is improved in the 1.5-km

This research is supported by United Kingdom NERC Changing Water Cycle programme grant NE/I006680/1

Steven C. Chan
School of Civil Engineering and Geosciences, Newcastle University, Newcastle upon Tyne, UK.
(*visiting scientist at the Met Office Hadley Centre)
Tel.: +44-1392-884802
Fax: +44-1392-885681
E-mail: steven.chan@metoffice.gov.uk

Elizabeth J. Kendon
Met Office Hadley Centre, Exeter, UK.

Hayley J. Fowler
School of Civil Engineering and Geosciences, Newcastle University, Newcastle upon Tyne, UK.

Stephen Blenkinsop
School of Civil Engineering and Geosciences, Newcastle University, Newcastle upon Tyne, UK.

Christopher A. T. Ferro
College of Engineering, Mathematics and Physical Sciences, University of Exeter, Exeter, UK.

David B. Stephenson
College of Engineering, Mathematics and Physical Sciences, University of Exeter, Exeter, UK.
Met Office Hadley Centre, Exeter, UK.

simulation, the 1.5-km simulation has a poorer mean bias with too many events exceeding high thresholds. Spatial density and clustering of summer extremes in the south-east England are poorly simulated in both the 12-km and 1.5-km simulations. In general, we have not found any clear evidence to show that the 1.5-km simulation is superior to the 12-km simulation, or vice versa at the daily level.

Keywords High resolution models · Dynamical downscaling · Hydroclimate · Precipitation

1 Introduction

With ever increasing computing power, dynamical climate model simulations can be performed at unprecedented high resolutions. There are many apparent benefits to high resolutions - most notably in the better representation of coastlines and topography. However, many atmospheric processes remain unresolved and require parametrisation, for example convection and cloud systems (Arakawa, 2004). Parametrisation schemes, in particular the cumulus convection scheme (Molinari and Dudek, 1992; Hohenegger et al, 2008), are often designed for coarser resolutions and may become less valid at increasingly high resolution. Molinari and Dudek (1992) argue that assumptions for traditional convective schemes begin to break down at horizontal resolutions of about 50 km. Therefore, an improvement in the representation of atmospheric processes by solely increasing resolution is far from certain.

Despite the high importance of accurate precipitation projections (in terms of social and economic impact), precipitation is among the most challenging climate variables to model, as precipitation is dependent on the representation of a wide range of processes. Precipitation can be caused by local convective instability, forced ascent near elevation changes, and synoptic variability ("weather patterns"), and relies on a number of model parametrisation schemes (e.g. convection, land-surface, boundary-layer, and cloud micro-physics schemes) for its representation in dynamical models. The modelled behaviour of these processes is likely to respond differently to resolution changes.

The varied geography of Britain leads to significant precipitation variations in a relatively small area (Wigley et al, 1984). Due to the different precipitation processes (orographic, convective, and synoptic-scale depressions) that are involved, one may expect a range of model sensitivities to horizontal resolution across the UK. Thus the UK provides a good test platform for assessing the precipitation sensitivity to model resolution.

There have been many studies testing model sensitivity to resolution changes considering various atmospheric and hydroclimate fields, with changes in mean bias and variance often used as the metric to assess model skill. Giorgi and Marinucci (1996) suggest that changes in topographic representation with resolution are the main cause of model sensitivity. Antic et al (2006) further argue that such sensitivity tends to lead to an improvement in the simulated climate. However, Laprise et al (2008) shows that while downscaling to higher resolution does tend to increase spatial variations (i.e. high spatial resolution fine features), the spatial variance increases are sensitive to domain size and do not necessarily improve deterministic skill (skill in simulating specific events) even if the climate representation is improved (overall statistics from the accumulation of many events).

69 Increase of inter-annual variability with increasing horizontal resolution from 50
70 km to 25 km is noted in Rauscher et al (2010); the same study also finds that
71 resolution increases lead to a reduction of the ratio of convective to total precipi-
72 tation and an improvement in seasonal precipitation over topographically complex
73 regions. For Britain, the 25-km simulations showed a marked improvement in the
74 spatial patterns of JJA precipitation.

75 The above work tends to focus on regional simulations that are of relatively
76 coarse resolution (25+km). Molinari and Dudek (1992) argue that some convective
77 processes begin to be partially resolved by the model at resolutions of about 20 –
78 25km. Over the UK, however, grid scales of ≈ 1 km are needed to give a satisfactory
79 representation of the majority of convection (Roberts and Lean, 2008), although
80 even at this scale not all convection is fully resolved. Such 'convection-permitting'
81 resolutions are now commonly used for short-term weather forecasting, and these
82 have shown considerable improvements in the representation of convective and
83 topographically enhanced precipitation (Roberts and Lean, 2008; Roberts et al,
84 2009). There are relatively few studies applying such high resolutions for longer-
85 term climate simulations, and such studies tend to be limited to a small domain or
86 a given season (Hohenegger et al, 2008; Wakazuki et al, 2008; Knote et al, 2010).
87 In this study, we assess the first 17-year extended length climate simulation at
88 convection permitting scales over a region of the UK.

89 High resolution climate models typically span a limited area, and are forced at
90 the lateral boundaries by reanalyses or a coarser-resolution global climate model
91 (GCM). The regional climate/mesoscale model (RCM) develops its own local cli-
92 matology in the interior of the domain, conditional on these lateral boundary
93 conditions (LBCs). In a one-way nesting approach, which is typically used, the
94 RCM does not feed information back to the driving model, with the assumption
95 that the regional model does not diverge strongly from the driving model in terms
96 of its representation of the large-scale conditions. The higher resolution RCM only
97 aims at adding information to what is not resolved by the driving model (Jones
98 et al, 1995, 1997). An obvious alternative to the one-way nesting approach is the
99 more computational expensive two-way nesting, in which the higher resolution -
100 smaller domain model interacts with the lower resolution - larger domain model.
101 Similar to two-way nesting, variable resolution stretched grid models can be em-
102 ployed, where the modeller uses higher horizontal resolution in regions of interest
103 (Déqué and Piedelievre, 1995).

104 The question that we seek to answer in this paper is “Does increasing model
105 resolution lead to a better representation of the character of intense precipitation
106 events?” While changes of variance and means are important, changes in the fre-
107 quency and intensity of precipitation extremes are of equal concern as well, due to
108 their relevance to floods and droughts. Model representation of event frequency,
109 intensity, and extremes is far more important than the mean in a social and eco-
110 nomic context (Meehl et al, 2000). Low probability “tail” extreme events are rare
111 such that their contributions to the climatological mean are comparatively small.
112 However, they may contribute strongly to inter-annual variations and anomalies
113 for specific years. The social impact of such events also depends on local geography,
114 antecedent hydroclimate conditions (i.e. soil moisture and groundwater levels) and
115 mitigation measures (i.e. flood and drought management). Furthermore, changes
116 in the mean do not always reflect changes in such rare “tail” events (Allen and
117 Ingram, 2002; Allan et al, 2010). Over the UK, regional climate models have been

118 shown to project increases in the magnitude of extreme rainfall events (Fowler
 119 et al, 2007; Fowler and Ekström, 2009). Characterising the sensitivity of extreme
 120 rainfall events to model resolution changes is thus important.

121 In this study, we seek to understand the sensitivity of simulated extreme rainfall
 122 to horizontal resolution using high resolution regional climate simulations carried
 123 out with the Met Office Unified Model. In particular, we compare 50-, 12-, and
 124 1.5-km simulations. The 1.5-km simulation corresponds to the first extended cli-
 125 mate simulation at convection-permitting scales over a region of the UK (southern
 126 UK, hereby SUK). We focus on precipitation events over SUK using the following
 127 metrics:

- 128 – Extreme event occurrences - in both space and time
- 129 – Intensities of such events
- 130 – Spatial organization and density (as in the expected number of events per grid
 131 box, see Appendix) of such events

132 We do not limit ourselves here to only rare events (such as daily precipitation
 133 heavier than 50 + mm/day), and also consider events that are more “moderate”
 134 (20 + mm/day). This study complements Kendon et al (in press), which analysed
 135 the same set of simulations. In summary, Kendon et al (in press) have found
 136 that the 12-km RCM precipitation tends to have lighter, more widespread and
 137 persistent precipitation relative to the 1.5-km RCM. The 1.5-km RCM is also found
 138 to have a better diurnal cycle. Here we focus only on daily precipitation (which
 139 is in contrast with the hourly precipitation focus in Kendon et al (in press)). The
 140 analyses here uses different metrics, and are seasonally and regionally stratified.
 141 Data from an additional 50-km RCM is also included.

142 This paper is divided into eight sections. In section 2, we present an overview of
 143 the modelling system and observational data that we have used. We then present
 144 our analysis methodologies in section 3. In sections 4 to 7, we compare the dif-
 145 ferences between the model simulations and observations with the use of different
 146 metrics. Finally, we conclude and discuss our results in section 8. There is also an
 147 appendix that discuss our methodologies in more detail.

148 2 Regional modelling system and observations used

149 Our simulations follow Kendon et al (in press) with the addition of a 50-km sim-
 150 ulation. Here we analyse data for the period 1991 to 2007 from the three different
 151 resolution (50km, 12km, and 1.5km) RCM simulations. All three simulations are
 152 different configurations of the Met Office Unified Model. An overview of the three
 153 simulations is presented in Table 1.

154 2.1 50-km and 12-km HadGEM3-RA

155 The 50-km and 12-km simulations are limited area versions of the non-hydrostatic
 156 Hadley Centre Global Environmental Model version 3 (HadGEM3-RA) (Walters
 157 et al, 2011). The model dynamical core uses a semi-implicit semi-Lagrangian
 158 scheme to solve the non-hydrostatic and compressible dynamical equations (Davies
 159 et al, 2005). The model uses a staggered Arakawa-C horizontal grid (Arakawa and

160 Lamb, 1977), and has 63 Charney-Phillips terrain-following hybrid vertical levels
161 (Charney and Phillips, 1953). The higher resolution 12-km simulation uses a
162 shorter time-step than the 50-km simulation (see Table 1).

163 Both simulations use the Met Office mass-flux CMOFS 4A convection scheme
164 (Gregory and Rowntree, 1990), the updated Wilson and Ballard (1999) cloud
165 microphysics scheme for large-scale precipitation (LSP) without prognostic rain,
166 and the Wilson et al (2008) PC2 prognostic cloud scheme. For the land surface,
167 the Met Office Surface Exchange Scheme 2.2 (MOSES2) (Essery et al, 2001) is
168 employed. For sea surface temperatures (SSTs), we have prescribed observed high-
169 resolution 0.25° daily SSTs (Reynolds et al, 2007).

170 Both simulations are forced by the ERA-Interim reanalysis (Dee et al, 2011) at
171 the lateral boundaries. The ERA-Interim has a T255 ($\approx 0.75^\circ$ or $\approx 80\text{km}$) spatial
172 resolution and 60 hybrid vertical levels. Temporally, the (re-gridded) reanalysis is
173 prescribed to the lateral boundaries every 6 hours. An illustration of the simulation
174 domain is shown in Fig. 1a. The simulation domain covers Europe and parts of
175 North Africa with the United Kingdom about a third of the way from the western
176 boundary.

177 2.2 1.5-km RCM

178 The 1.5-km regional climate model uses a modified version of the non-hydrostatic
179 Met Office operational UK variable-resolution model (UKV). Like the HadGEM3-
180 RA, UKV is also one of the configurations of the Met Office Unified Model. It
181 has a grid spacing of 1.5km in the interior with a transition to 4-km at the edges.
182 This gives a 1 : 3 downscaling ratio near the boundaries. This variable resolution
183 rim reduces instabilities near the lateral boundaries. The operational 1km UKV
184 has been shown to improve UK orographic and convective precipitation relative
185 to coarser 12km simulations (Roberts et al, 2009; Roberts and Lean, 2008; Lean
186 et al, 2008).

187 The majority of the model physics in the 1.5-km simulation is the same as
188 in the 12-km and 50-km simulations, but there are some important differences.
189 Similar to the 50-km and 12-km HadGEM3-RA simulations, the 1.5-km simula-
190 tion shares the same dynamical core (Davies et al, 2005). The same land surface
191 (Essery et al, 2001) scheme and prescribed SSTs are used in all three simulations.
192 Unlike the coarser simulations, however, the 1.5-km simulation uses no convective
193 parametrisation, nor the prognostic cloud scheme (see Kendon et al (in press) for
194 details). Time stepping and the number of vertical levels also differ (see Table 1).
195 The 1.5-km simulation uses the (Wilson and Ballard, 1999) cloud microphysics
196 scheme with prognostic rain. The Smagorinsky-Lilly model (Smagorinsky, 1963;
197 Lilly, 1962) is used to represent sub-grid turbulent diffusion.

198 The simulation is driven by the 12-km RCM simulation, with no feedback
199 from the 1.5-km simulation back to the 12-km simulation ('one-way nesting'; see
200 section 1). Unlike the two coarser resolution simulations, the 1.5-km RCM domain
201 is limited to SUK (see Fig. 1b) where convective events are observed to be the
202 most common in Britain. Due to the small size of the 1.5-km domain, we expect
203 strong similarities in the regional atmospheric conditions between the 1.5-km and
204 12-km simulations over the SUK. For inter-comparisons, we upscale the 1.5-km
205 simulation results to the 12-km and 50-km scale.

2.3 Observations

The National Climate Information Centre daily UK gridded precipitation (Perry et al, 2009) is used as a reference to compare all three model simulations. The daily gridded dataset begins in 1958 and ends at the present day, and here we use data from 1991 to 2007. Between 1991 and 2007, the dataset has used approximately 2500-3500 surface gauge observations that are scattered over England, Wales, Scotland, and Northern Ireland. Approximately two-thirds of these gauges are in SUK.

Quality control is performed through computerized and manual comparisons of individual daily station values against the daily all-station average and daily values from nearby stations. Any stations that have failed quality control are excluded from the computation of the gridded values. The gridding of the gauge data to a $5\text{km} \times 5\text{km}$ grid uses a cubic inverse-distance weighting interpolation using stations within 50km radius of the grid box.

There are three notable issues for such a dataset:

- Values are undefined over water;
- Station gauge observations can only sample events that occur over the gauges themselves, and may not sample specific localized events;
- Gauges are often located in valleys, and that leads to an underestimation of precipitation in the vicinity of high topography;

To address the first issue, we restrict all our comparisons to land points only. The second and third issues are fundamental limitations to rain gauge data - one can only detect local events if they are sampled by the gauges. The under-sampling of convective and orographic precipitation extremes will cause the area averaged gridded values to be less than the true area-averaged value. Ensor and Robeson (2008) show that gridded gauge precipitation produces reasonable annual precipitation estimates, but selectively degrades the representations of high and low precipitation events.

We intend to investigate this problem in further detail in the near future with other observation datasets (see section 8). We expect the problem is more likely to affect rare (once every few years) localized extremes. Such extremes are more common in JJA when localized convection is the most common. During DJF, the under-sampling is expected to be lesser of a problem as extremes are more associated with large-scale precipitation.

3 Methodologies

In order to compare between model simulations and daily observations, we have re-gridded our observations and model simulations to the 12-km and 50-km grid:

- The 1.5-km simulation is upscaled to both 12-km and 50-km scales when compared against the 12-km and 50-km simulations;
- The 12-km simulation is upscaled to the 50-km scale when compared against the 50-km simulation;
- The 5-km gridded observation dataset is upscaled to the 12-km and 50-km grids.

249 Since we are only interested in days that have (significant) precipitation events,
 250 we only include days with events exceeding given minimum thresholds. The ex-
 251 amined thresholds are: 1.0, 5.0, 10.0, 20.0, 30.0, 40.0, and 50.0mm/day. We also
 252 estimate spatial scales and the clustering of precipitation events with the Ripley
 253 K-function (Ripley, 1977). A description of the Ripley K-function can be found in
 254 the appendix.

255 Both parametric and non-parametric statistical significance tests are used in
 256 our analysis. For basic comparisons between climatological seasonal means, we
 257 have employed the Student-T test at the 5% level. Since there are 17 years of
 258 data, the degrees of freedom for the Student-T test are $dof = 17 - 1 = 16$.

259 For the comparisons between event intensities, we have used a 1000 member
 260 bootstrap (Efron and Tibshirani, 1993; Wilks, 1997), and test at the 10% sig-
 261 nificance level. We define a precipitation subset (P') in which a daily threshold
 262 ($p_{\text{THRESHOLD}}$) has been exceeded (Equation 1). The average event intensity ($\langle P' \rangle$)
 263 is defined to be the expected daily intensity within the subset (Equation 2):

$$264 \quad P' = \{P \geq p_{\text{THRESHOLD}}\} \quad (1)$$

$$\langle P' \rangle = \frac{\sum_{n=1}^{N(p_{\text{THRESHOLD}})} P'_n}{N} \quad (2)$$

$$265 \quad N(p_c) = |P'| \quad (3)$$

266 In which P is the set of all non-zero precipitation values. N is the number of
 267 elements in subset P' . Both P' and N are functions of $p_{\text{THRESHOLD}}$. P can be
 268 a set that is formed all values for all grid points (as in Figs. 6 and 7) or at each
 269 individual grid point (as in Figs. 4 and 5 in which we have denoted event counts
 270 (per year) at each grid point as n).

271 $\langle P' \rangle$ can be computed with the original dataset and a bootstrap. The bootstrap
 272 re-sampling is performed in 3-month seasonal blocks for each year (e.g. 1991 JJA,
 273 1992 JJA, ..., 2007 JJA). We randomly select 17 seasons (out of the total of 17
 274 years) with replacement, such that some years may be represented more than
 275 once and some not at all. We re-sample in seasonal blocks to account for possible
 276 auto-correlation. Wilks (1997) suggests that the block length can be estimated
 277 through independent sample number estimation assuming the process is a 1st-
 278 order autoregressive process. Such estimation is difficult practically as the auto-
 279 correlation of daily precipitation is caused by a number of mechanisms which act
 280 at a range of time scales: from 1-5 day synoptic variations to soil-precipitation
 281 feedbacks that operate over time scales of weeks and months. A seasonal block
 282 assumes that the precipitation intensities from the same season of the previous year
 283 to be independent of the precipitation intensities of the present season. Generally,
 284 long block sizes lead to Type-II errors - not enough null hypothesis rejections (i.e.
 285 significance tests favour higher probabilities for null hypothesis for non-difference
 286 between models and observations) (Wilks, 1997).

287 The re-sampling procedure is repeated 1000 times to produce 1000 simulated
 288 17-season datasets. The original dataset is one out of $\binom{2n-1}{n}$ (for $n = 17$, $\binom{2n-1}{n} \sim$
 289 10^9) possible outcomes from the re-sampling. For each bootstrap, we compute
 290 the intensity differences between the two compared datasets. The null hypothesis
 291 is that the differences are zero. We estimate the top and bottom 5% percentile
 292 (corresponding to a two-tail 10% significance test) of the 1000 differences from

293 the bootstrap, and check if the top (or bottom) 95% differences have same signed
 294 differences. If the sign is the same, we reject the null hypothesis.

295 4 Simulated climatologies

296 We first examine the difference in precipitation climatologies between the obser-
 297 vations and models. This also serves as an introduction to the UK climate for
 298 unfamiliar readers. Shown in Fig. 2 and Fig.3 is the observed 3-month seasonal
 299 mean precipitation (and the three model-simulated fractional departures from the
 300 observed values) at both the 50-km and 12-km scale.

301 For all seasons, observed precipitation is highest over the Welsh mountains
 302 and south-west England. Lower amounts are observed in the lowlands to the east.
 303 Therefore for further analysis, we divide our SUK domain into two sample regions
 304 using the “Tees-Exe Line”¹ (see Fig. 1b). This line separates the meteorologically
 305 wetter and topographically higher north west (NW) and the meteorologically drier
 306 and topographically lower south east (SE). The models (at all three resolutions)
 307 tend to have negative (positive) precipitation bias over the NW (SE). However,
 308 the biases show seasonal variations, which are similar for all three simulations.

309 The Tees-Exe Line also separates the east which is subject to relatively more
 310 intense local extremes than the west. To the east of the line, the 100-year-return
 311 level event is on average 2.5 – 3.2 times more intense than the 2-year-return level
 312 event², while the same ratio is lower (2.0 – 2.5) to the west of the line (Faulkner,
 313 1999).

314 The observations show that SON (MAM) is the wettest (driest) three-month
 315 period for SUK. JJA and DJF, which we will examine in detail here, have precipi-
 316 tation amounts in between SON and MAM. JJA and DJF are chosen for thorough
 317 analysis as they represent two different precipitation regimes: primarily convective
 318 rain concentrated to the east of the Tees-Exe Line during JJA, and frontal precipi-
 319 tation concentrated to the west during DJF (Maraun et al, 2009). Over highland
 320 regions, DJF precipitation is higher than JJA. Over the lowlands, the highest
 321 JJA precipitation values are lower than the highest DJF precipitation values over
 322 Southern England; however, over eastern England and East Anglia, JJA is wetter
 323 than DJF. For the models, the NW dry bias is largest during SON and DJF when
 324 highland precipitation is higher, and the SE wet bias is largest during MAM when
 325 lowland precipitation is highest.

326 By examining Fig. 2 and Fig. 3, it appears that increasing the model resolution
 327 has a positive impact on orographic precipitation in the NW. When resolution is
 328 increased from 50-km to 12-km, the (negative) bias over Wales is reduced. Mi-
 329 nor reductions of positive bias are noticeable in the SE. Even though the 1.5-km
 330 simulation is driven by the 12-km simulation, the patterns of their bias differ sig-
 331 nificantly - the 1.5-km simulation is notably wetter than the 12-km simulation.
 332 Positive biases over the SE are higher in the 1.5-km simulation. The 1.5-km simu-
 333 lation does show (negative) bias reduction for orographic precipitation over Wales
 334 for SON and MAM. This improvement in orographic precipitation is consistent
 335 with what has been found in previous studies (see section 1).

¹ The line joining the mouths of the River Exe and the River Tees in UK

² Often called the “growth rate” in hydrology.

336 For the SE, there appears to be little value in going to a higher model reso-
337 lution; in fact, results here in terms of seasonal mean precipitation show that the
338 resolution increase has a negative impact on the bias. These results are consistent
339 with Kendon et al (in press), and the excessive precipitation in the 1.5-km model
340 is thought to be due to the inherent under-resolving of convection at the 1.5-km
341 scale. However, we will show that resolution increases lead to changes in other
342 important precipitation statistics.

343 5 Localized event frequencies

344 The climatological mean (and model biases in the mean) does not convey any
345 information about the frequency and intensity of events. To begin our discussion,
346 we have plotted the observed and simulated annual June-November (JJA+SON)
347 and December-May (DJF+MAM) occurrences of precipitation events exceeding
348 20mm/day (Fig. 4) and 50mm/day (Fig. 5). We have plotted frequencies on both
349 the 12-km and 50-km grid. The use of half year divisions is based on the similarities
350 of occurrence frequencies between JJA and SON and between DJF and MAM
351 (not shown). We expect the frequencies of these types of events to increase with
352 decreasing grid size (evident when comparing panels a against d, and c against e
353 in both figures). At a coarse grid size (i.e. the 50-km grid scale), area averaging
354 favours events that are widespread as localized convective events are filtered out
355 by area averaging.

356 Both observations and models indicate that one may expect between 1-10 20 +
357 mm/day events per year (JJA+SON and DJF+MAM) at the 12-km and 50-km
358 grid scale with the highest frequencies over the western part of our domain. On
359 the east side of the Tees-Exe Line, event frequencies at both thresholds are higher
360 in JJA+SON than in DJF+MAM, but such seasonal variations are not as evident
361 over Wales and south-western England. All models captured the higher frequency
362 of event occurrences observed over Wales, the east-west gradient of the frequency,
363 and the seasonal variations in the south-east.

364 Frequencies for 20 + mm/day events are higher everywhere for the 1.5-km (12-
365 km) simulation in SUK when compared with the 12-km (50-km) simulation. For
366 the 1.5-km simulation, the increase in the number of events is most evident along
367 the southern and south-eastern England coast in both JJA+SON and DJF+MAM,
368 and the increased frequencies are higher than the observed estimates. The increase
369 of 20 + mm/day event frequencies in the 12-km simulation (when compared with
370 the 50-km simulation) occurs both to the west and the east of the Tees-Exe Line.
371 The 12-km simulation is also superior to the 50-km simulation in terms of capturing
372 the high frequencies over the Welsh highlands.

373 As one moves to the 50 + mm/day threshold, event occurrences decrease (Fig.
374 5). Typically there are no more than 1-2 events per year (JJA+SON and DJF+MAM)
375 at any grid point for the 17 years of analysed data (sometimes just once within
376 all 17 years of data; the 0.025 events/year contour in Fig. 5 is chosen based on
377 $\frac{1}{17} \times \frac{1}{2} \approx 0.025$). Similar to the 20 + mm/day threshold, observations show an east-
378 west gradient in occurrence number with the highest frequencies observed over the
379 Welsh highlands. In the 50-km simulation, there are too few 50 + mm/day events
380 to discern such a gradient. The southern / south-eastern coast event increase that
381 is evident at the 20 + mm/day threshold within the 1.5-km simulation is also evi-

dent at the 50 + mm/day threshold for both JJA+SON and DJF+MAM, leading to an increased bias with respect to observations.

Given the above analysis, there is a clear improvement in the model simulation of the occurrence of heavy precipitation when model resolution is increased from 50-km to 12-km in both the orographic regime to the west and lowland regime to the east. However, there is little value of increasing the resolution from 12-km to 1.5-km as biases worsen. However, Figs.4 and 5 convey no information about spatial structures and average intensities of 20 + mm/day and 50 + mm/day events.

6 Excess intensity and event-based statistics

In this section, we examine the average intensity ($\langle P' \rangle$, see Equation 3) of events exceeding various thresholds from 1mm/day to 50mm/day. The results are presented in Fig. 6 and Fig. 7 for JJA and DJF respectively. As in previous figures, results are presented with data that are upscaled to 50-km (left panels) and 12-km (right panels). We have plotted up to the 50mm/day threshold due to the rarity of 50 + mm/day events in the 50-km simulation (as indicated in panel c of both figures).

6.1 JJA

At the 12-km grid scale, in both the SE and NW subregions, the 12-km simulation simulates precipitation intensities that are 10% – 20% higher than observations for thresholds above 30mm/day, and the differences are statistically significant at the 10% level. The 1.5-km simulation simulates a lower and closer-to-observation intensity for the same 30 + mm/day thresholds. When the comparisons are made at the 50-km scale, both the 12-km and 1.5-km simulations show SE intensities that are 5-10% higher than observations.

For lower thresholds (below 10mm/day, where all events above this threshold are included), only the 1.5-km simulation has higher ($\approx 20\%$ for the SE) average intensity than the observations. That is true for both the NW and SE subregions. The other two (12-km and 50-km) simulations have either intensities that are lower (NW) or that are not statistically different (SE) from observations.

The 50-km model simulation underestimates event intensities. Over the NW, this underestimation is significant for events exceeding thresholds up to 30mm/day, and becomes insignificant at higher thresholds. By contrast over the SE, this underestimation only becomes significant at higher thresholds (40mm/day and 50mm/day).

6.2 DJF

DJF precipitation intensities are better simulated by the 12-km and 1.5-km simulations than by the 50-km simulation, with the negative intensity bias in the NW reduced or eliminated entirely in the higher resolution simulations. The 50-km simulation has consistently lower intensities in the NW than observations; differences at all but one threshold (40mm/day) are statistically significant at the 10% level.

422 For the 12-km simulation, intensities of higher threshold NW events are well sim-
423 ulated at both the 12-km and 50-km scale, and are not statistically different from
424 observations at any threshold above 10mm/day. Unlike the 12-km simulation, the
425 1.5-km simulation tends to show positive biases of about 5% – 10% across multiple
426 thresholds when the data is upscaled to the 12-km scale. At the 50-km scale, the
427 1.5-km simulation has positive biases in two (20mm/day and 40mm/day) out of
428 seven thresholds.

429 At lower thresholds (below 10 + mm/day), all three simulations have lower
430 NW intensities than observed at the 50-km grid scale. The biases are reduced
431 for the 1.5-km and 12-km simulations if the comparisons are made at the 12-km
432 scale. Since the differences disappear or are reduced at higher thresholds (above
433 10mm/day), this shows that all simulations have deficiencies in the simulation of
434 moderate events (1 – 10mm/day).

435 SE precipitation intensities that are simulated by the 50-km and 12-km sim-
436 ulations are not statistically different from observations. The 1.5-km simulation
437 simulates higher intensities in the SE at both 12-km and 50-km grid scale. In Fig.
438 3, it is notable that the 1.5-km simulation also has the highest SE DJF positive
439 bias among the three simulations.

440 6.3 Event occurrences as a function of intensity threshold

441 Total event numbers (across all grid boxes and days) are shown in the lower panels
442 (c,d) in both Fig.6 and Fig. 7. The number of events decreases with increasing
443 intensity threshold, as would be expected, and the decrease rates are highest for
444 the 50-km simulation. The number of NW and SE 1+mm/day events is comparable
445 for all model resolutions and observations, but the number of 40 + mm/day events
446 in the 50-km simulation is up to an order of magnitude less than the two other
447 simulations and observations.

448 Panels Fig. 6 c,d and Fig. 7 c,d are integrated measures of event occurrence
449 in both time and space. In order to partition out temporal occurrences, in Table
450 2, we present the number of days which have at least one event greater than the
451 threshold at the 12-km scale. For the 50-km scale (not shown), higher (40mm/day
452 and 50mm/day) threshold events are lacking especially for the 50-km simulation.

453 For JJA (Fig. 6 c,d), the total number of events in the 50-km simulation and the
454 observations are consistently lower than in the 12-km and 1.5-km simulations for
455 thresholds above 40mm/day. However, we expect the estimated observed counts
456 to be lower than the true value (see section 2.3), so the positive event number
457 biases in the 12-km and 1.5-km simulations may be less than shown. The 50-km
458 simulation itself has less counts than the observations; using the same argument
459 as above, the underestimation by the 50-km simulation may actually be higher
460 due to under-sampling by the observations. A comparison between Table 2 and
461 Fig. 6 indicates that in the 1.5-km simulation the excessive number of events is
462 partially due to the large number of days having at least one event somewhere
463 in the SUK domain. For the 12-km simulation, results are more curious as the
464 number of days having at least one event is less than in the observations until the
465 50 + mm/day threshold. We shall show that the spatial density of events is the
466 cause of the discrepancy.

467 For DJF, the 1.5-km and 12-km simulations are more realistic than the 50-
 468 km simulation in simulating the number of events over the mountainous NW,
 469 especially with thresholds of 30 + mm/day or higher. At the 12-km scale, the
 470 1.5-km simulation has 2 – 5 times more SE events than the observations for the
 471 30 + mm/day and 40 + mm/day thresholds. It is worth noting that such heavier
 472 SE DJF precipitation events are rare when compared with JJA, and the number
 473 of DJF events for the whole domain (SE + NW) is mostly attributable to the NW.
 474 All three model simulations are able to capture that NW-SE difference.

475 6.4 Section summary

476 Here are some of the key results from this section:

- 477 – Both the 12-km and 1.5-km simulations and observations have higher precip-
 478 itation intensities and event numbers than the 50-km simulation in both JJA
 479 and DJF;
- 480 – The 1.5-km simulation has more realistic intensities for JJA intense precipita-
 481 tion events than the 12-km simulation;
- 482 – The 12-km simulation has more realistic intensities for DJF intense precipita-
 483 tion events than the 1.5-km simulation;
- 484 – The 1.5-km simulation has a larger number of events than the other two model
 485 simulations and observations across many thresholds;
- 486 – For most thresholds above 20mm/day, the 12-km (1.5-km) simulation has fewer
 487 (more) days in JJA with at least one precipitation event in the SUK domain
 488 compared to observations.

489 Our results indicate that the 50-km simulation performs least well in compar-
 490 ison to the higher resolution simulations in simulating intense daily precipitation.
 491 However, a mixed picture is shown between the two higher resolution simulations.

492 7 Spatial density and clustering

493 We have presented the temporal occurrences of intense precipitation events; and
 494 in this section, we examine the spatial characteristics of intense daily precipitation
 495 events. Clustered local precipitation events pose a larger risk than scattered events
 496 in triggering flooding. Thus the realistic simulation of the spatial characteristics
 497 of precipitation is essential for using models as a flood risk assessment tool.

498 Using the NW and SE regional division, we compute the average spatial density
 499 (Tables 3 and 4)³, the number of near neighbours, and spatial clustering. The
 500 *spatial density* is the total number of precipitating grid points with the threshold
 501 exceeded divided by the total number of defined grid points (see Equation 5 in
 502 Appendix). The spatial density can then be averaged across all days that have at
 503 least 2 grid points that have exceeded the threshold (see Equation 17 in Appendix).

504 *Clustering* is a localized (an area subset of the whole domain) density enhance-
 505 ment (excess density above the average density of the whole domain). Density and

³ Only 1.5-km model simulated SE DJF 50 + mm/day event statistics are shown due to the lack of events in the other datasets.

506 clustering are two different concepts; clustering may exist in the absence of “high”
 507 densities. A schematic that illustrates the differences between density and cluster-
 508 ing is shown in Fig. 8. As in density, we present the time average values only (see
 509 Equations 18 and 19 in Appendix).

510 Clustering is assessed by calculating the area normalized Ripley K-function
 511 (also known as the Besag L-function; see appendix) of precipitation events exceed-
 512 ing two specific thresholds (20 + mm/day and 50 + mm/day). High spatial den-
 513 sity values may arise from many individual disorganized single grid-point showers
 514 (with low clustering) or many clustered “precipitation blobs” (non-zero Besag L-
 515 function). The results are presented in Fig. 9 and Fig. 10 for JJA, and Fig. 11 and
 516 Fig. 12 for DJF. Shown are:

- 517 – The estimated number of near neighbours⁴ and Besag L-function assuming
- 518 events are not clustered (left panels, dash line)
- 519 – The actual number of near neighbours (left panels, solid line) and Besag L-
 520 function as observed in the gridded observations (right panels), 12-km and
 521 1.5-km simulations

522 In a nutshell, the right panel (Besag L-function) measures the excess of clus-
 523 tered points (left panels, solid lines) above the background (left panels, dashed
 524 lines).

525 Here we limit our comparisons to only the 12-km horizontal scale. This is
 526 because coastlines and island geography become too coarse at the 50-km scale,
 527 and the poor simulation of rare high-intensity events by the 50-km model. For
 528 example, East Anglia and Cornwall-Devon are only 1-3 grid points wide at the
 529 50-km scale (see Fig. 2).

530 7.1 JJA

531 In general, the clustering and spatial density are much better simulated in the
 532 NW than in the SE by both simulations. For the NW, both models are reasonably
 533 successful in simulating the average clustering at both thresholds (Figs. 9 a and 10
 534 a, dashed lines). Naturally, clustering over the NW is tied with orography, and a
 535 better simulated clustering in the NW is not surprising. The 20 + mm/day events
 536 are also better handled than the 50 + mm/day events.

537 By comparison with the NW, both models are more challenged to simulate
 538 the spatial density and clustering over the SE. Figs. 9 and 10 (lower panel c,
 539 dashed lines) show that both the 12-km and 1.5-km simulations tend to simulate
 540 precipitation that is spatially too dense at both thresholds in the SE. Both models
 541 are more successful in reproducing the observed clustering at the 20 + mm/day
 542 threshold (Fig. 9 d) than at the 50 + mm/day (Fig. 10 d). For the 50 + mm/day
 543 threshold, there is severe underestimation of clustering in the SE, but the same
 544 is not evident at the 20 + mm/day threshold. In general over the SE, the 12-km
 545 simulation gives a better representation of the average spatial density than the
 546 1.5-km simulation, whilst the 1.5-km simulation gives a better (but still poor)
 547 representation of clustering for the 50 + mm/day threshold.

⁴ The average spatial event density multiplied by the surface area

548 The excessive density in the 12-km simulation over the SE at the 20 + mm/day
 549 threshold compensates for the reduced number of days of event occurrence - leading
 550 to an overall comparable total number of events between the 12-km simulation and
 551 observations (Fig. 6 d). For 50 + mm/day events, both too many days with events
 552 and the excessive spatial density contribute to the excessive number of events in
 553 the 12-km and 1.5-km simulations.

554 We note that observed clustering peaks at around 4-10 grid points (for both
 555 thresholds) in the SE. This is consistent with length scales of organized mesoscale
 556 convective events ($\approx 10^1 - 10^2$ km).

557 7.2 DJF

558 Relative to JJA, both models generally show much better skill in simulating the
 559 spatial densities and clustering in DJF. For the DJF 20 + mm/day threshold (Fig.
 560 11), the SE clustering (panel d) in the 12-km and 1.5-km simulations is similar,
 561 with both simulations tend to underestimate observed clustering at “large” ($r \geq 10$
 562 grid points) radii. The observed spatial density of 20+mm/day events is in between
 563 the values simulated by the 12-km and 1.5-km simulations in both NW and SE
 564 (panels a and c, dashed lines; Tables 3 and 4 column c). This is different to the
 565 situation in JJA, where both simulations have SE spatial densities that are too
 566 high relative to observations.

567 For 50 + mm/day events, the simulated clustering in the NW (Fig. 12b) is
 568 higher for both simulations (with the 1.5-km simulation closer to observations).
 569 This is in contrast with JJA (Fig.10 b) when the simulated clustering is lower
 570 than observed. Both simulations simulate spatial densities that are higher than
 571 observed (Fig. 12 a, dashed lines; Table 3 column d).

572 We have not shown the clustering and near neighbour number counts for DJF
 573 SE 50 + mm/day events for 2 out of the 3 datasets. There are only 1 and 3 DJF SE
 574 50 + mm/day events between 1991 and 2007 that have spatial scales more than 2
 575 or more grid points for the observations and 12-km model simulation respectively.
 576 The difference in the number of events can be seen in Fig. 5 j-l. The probability of
 577 having a 50+mm/day event in the SE during DJF+MAM is highest for the 1.5-km
 578 simulation with most events concentrated along the southern coast of England. In
 579 summary, the lack of DJF SE 50 + mm/day events in the 12-km simulation and
 580 observations is consistent with the event frequency differences between the two
 581 models and the observations.

582 7.3 Section summary

583 The above results reveal a few important points:

- 584 – With the exception of the 1.5-km model simulated NW DJF 20 + mm/day
 585 spatial density, all examined model simulated spatial densities are either higher
 586 or comparable to observations.
- 587 – Despite the higher spatial density, both simulations tend to underestimate
 588 spatial clustering of 50 + mm/day events over the SE in JJA.

589 Similar to the results for precipitation intensities, there are no clear improve-
590 ments to precipitation clustering and spatial density from increasing the model
591 resolution from 12 km to 1.5 km. The simulation of the SE during JJA has been
592 especially challenging for both simulations - overall spatial density is overesti-
593 mated for both thresholds, and spatial clustering (organization) of daily extremes
594 ($50 + \text{mm/day}$) is poor. Due to the nature of the observations, the observed cluster-
595 ing may be underestimated, and this suggests model discrepancies may be larger.
596 We note the above picture may change if different accumulation periods are ex-
597 amined (hourly or multi-hourly), and is suggested by the results in Roberts and
598 Lean (2008).

599 8 Discussions and Conclusions

600 We have presented a number of event-based metrics in this paper. These have been
601 chosen to gauge differences in the model simulations across different resolutions.
602 Key results include:

- 603 – Increasing model resolution from 50 km to 12 km is beneficial to the simu-
604 lation of DJF orographic precipitation. The 50-km simulation underestimates
605 the occurrence and intensity of heavy precipitation and has a negative mean
606 precipitation bias over orography. This is reduced in the 12-km simulation.
- 607 – Seasonal biases in precipitation totals increase when resolution is increased
608 from 12 km to 1.5 km.
- 609 – Moderate-to-heavy daily precipitation occurs too often in the 1.5-km simula-
610 tion - especially in SE England. The average intensity of the JJA (DJF) daily
611 extremes is better simulated by the 1.5-km (12-km) simulation. Both the 12-
612 km and 1.5-km simulations have too many days with extreme ($50 + \text{mm/day}$)
613 JJA precipitation.
- 614 – Both 12-km and 1.5-km simulations overestimate JJA spatial density of events
615 over the SE for two thresholds examined here ($20 + \text{mm/day}$ and $50 + \text{mm/day}$).
616 On top of the overestimation, there is clear deficiency for both simulations in
617 capturing the appropriate spatial clustering for SE JJA $50 + \text{mm/day}$ events.

618 In general, there are some improvements in simulating daily intense precipita-
619 tion when model resolution is increased from 50 km to 12 km. When resolution is
620 further increased to 1.5-km, there is no further clear cut improvement. Compar-
621 isons between the 12-km and 1.5-km simulation give a mixed picture: better JJA
622 daily extreme intensity in the 1.5-km simulation versus smaller seasonal biases in
623 the 12-km simulation in multiple seasons. We acknowledge that there are many
624 ways to compare model simulations, and one of the objectives of this study is
625 trying different ways to do the comparison.

626 Improved representation of precipitation in DJF over orography between the
627 50-km and 12-km is a result consistent with other similar studies (see section 1).
628 Our results indicate that boreal summer (JJA) precipitation away from orography
629 may or may not have benefited with increasing resolution depending on the metric
630 used.

631 The summer of SE UK represents the convective precipitation regime over UK.
632 The 1.5-km simulation shows an improvement over the 12-km simulation in the
633 simulation of average intensities of high threshold JJA events, but such events are

634 too common in the the 1.5-km model (event day counts are too high, Table 2).
635 Spatial clustering and density are deficient in both simulations especially at the
636 high thresholds.

637 Daily precipitation extremes are linked to multi-hour slowly moving (frontal or
638 convective) precipitating systems. Short duration and/or fast moving precipitation
639 systems do not lead to extreme daily accumulations (but they may be linked to
640 extremes at shorter time scales). The above argument suggests that a different
641 result may be obtained if the analysis is performed for accumulations over shorter
642 periods. The above also highlights that a good simulation of precipitation duration,
643 spatial organization and temporal evolution of precipitation systems is essential
644 to give reasonable extremes in the model climate.

645 The 12-km simulation has fewer JJA heavy precipitation days, and the 12-km
646 heavy events have a more “outbreak” nature than the 1.5-km simulation. The 12-
647 km simulation has less days with moderate-high precipitation. When moderate-
648 high daily precipitation events are triggered, they become overly intense (daily
649 totals are too high) and widespread (spatial density of grid points above a mod-
650 erate/high daily threshold is too high).

651 In JJA, for more moderate thresholds (20+mm/day), the 12-km model appears
652 to have the best simulated intensity. However, the 12-km simulation has nearly 20-
653 25% less days with any such events. Therefore, it is hard to conclude if the 12-km
654 simulation is any better than the 1.5-km simulation in simulating more moderate
655 daily events.

656 For the metrics that we have compared, the 12-km simulation appears to out-
657 perform the 1.5-km simulation in DJF. On the whole, boreal winter (DJF) heavy
658 precipitation is easier to simulate than boreal summer (JJA) precipitation. Simu-
659 lated intensities, spatial densities and clustering are all better simulated in DJF.
660 Our results indicate that there is no benefit in increasing model resolution higher
661 than 12 km for DJF for the used models within the context of regional climate
662 modelling. Similar results have been demonstrated for other regions of the globe
663 (Hong and Leetmaa, 1999). This is due to the dynamical processes that drive win-
664 ter precipitation events - caused by fronts and synoptic depressions with scales of
665 the order of $10^2 - 10^3$ km. That is 2-3 orders of magnitude larger than 1.5 km.

666 An important question remains unanswered - the value of increasing model
667 resolution above 12-km for JJA precipitation. Results presented here for daily
668 precipitation are mixed, but Kendon et al (in press) have shown clear improve-
669 ments when the same data is examined at the sub-daily time scale in metrics such
670 as diurnal variability, duration, and spatial extent. Many of the remaining biases
671 at 1.5 km may be explained by the fact that the 1.5-km simulation is “convection
672 permitting”; i.e. even at 1.5 km, convection is still under-resolved.

673 Our results indicate that the 1.5-km model simulates too many heavy precip-
674 itation events in JJA (too many event counts, spatial density that is too high).
675 This is a result consistent with Lean et al (2008). With convection under-resolved,
676 the explicitly-resolved convective motion and vertical mass flux become too in-
677 tense. That is because cloud-scale up- and down-drafts are still under-resolved
678 where grid box vertical motion is either all up or all down. This is in contrast with
679 CP-enabled model simulations where vertical convective motion is parametrised
680 under the presumption that cloud-scale convective motions (mixed between up
681 and downward motion) are not resolved, and the thermodynamical and dynamical
682 consequence of the unresolved convective motions are estimated and feedbacks to

683 the larger model resolved scale. The use of Smagorinsky-Lilly turbulent diffusion
684 (Smagorinsky, 1963; Lilly, 1962) has alleviated problems with convective showers
685 being too intense in the 1.5-km simulation. However, this is still an active research
686 area in “convective permitting” models. Another option is to increase resolution
687 yet further (e.g. to $\sim 10^2\text{m}$); this would lead to considerable increases in compu-
688 tational cost, and also the suitability of other model physics would then need to
689 be re-examined, especially the representation of the boundary layer and the land
690 surface scheme.

691 We have not discussed the sensitivity of our results to domain size and bound-
692 ary changes. Such sensitivity is well discussed in the literature (Jones et al, 1995;
693 Seth and Giorgi, 1998; Leduc and Laprise, 2009); that is large (small) domains give
694 the model greater (less) freedom to develop its own features. The current work can-
695 not explore such sensitivity, and running many high resolution RCM simulations
696 are computationally expensive. The 1.5-km RCM domain is $\sim 1000\text{km}$ wide - small
697 in comparison with the domain sensitivity study by Leduc and Laprise (2009). It is
698 intriguing to ask how such domain size sensitivity manifests itself in high resolution
699 RCM simulations. The last question should be explored in the future.

700 Gridded gauge observations may underestimate clustering, variance, and inten-
701 sity for specific events, particularly in summer when extremes are more localised.
702 In order to estimate the degree of underestimation of clustering and intensity of
703 local extremes in the observations, one requires independent high-resolution esti-
704 mates of daily/hourly precipitation. We intend to revisit this problem again in the
705 near future using radar and hourly gauge data (Golding, 1998).

706 We have not discussed inter-annual variability in this paper. Out of the 17
707 years that we have analysed (1991-2007), 2007 was a major flood year in the SUK
708 (Blackburn et al, 2008). The models do not capture the heavy rain in central and
709 western UK that was seen in observations (not shown). The 2007 UK floods were
710 caused by two synoptic events, whose tracks and precipitation patterns are not well
711 captured by the simulations despite the use of reanalysis data as lateral boundary
712 conditions. We note that, however, reanalysis information is only fed in at the
713 edge of the European domain, and one should not expect exact agreement in the
714 positioning of events over the UK - not only between models and observations,
715 but also between models themselves.

716 Any type of model projection for future climate change needs to be carefully
717 interpreted in the context of an understanding of model strengths and limitations.
718 Even with increases in model complexity (such as increasing the horizontal reso-
719 lution as shown here), many limitations can still exist in their simulations for the
720 current climate.

721 **Appendix: The Ripley K function**

722 The Ripley K-function (Ripley, 1977) is a measure of spatial clustering which com-
723 pares the number of near neighbours with the average spatial density of the whole
724 region of interest (Fig.3). Given any (time-varying) map (e.g. gridded precipita-
725 tion), one marks all the events with ones (1) and non-events with zeroes (0). We
726 denote that map (effectively a matrix/vector) with I :

$$I(x, y, t) = \begin{cases} 1, & \text{if } P \geq P_c \\ 0, & \text{if } P < P_c \end{cases} \quad (4)$$

727 , where P_c is the threshold. The average spatial density of the events is simply
728 defined as:

$$\varrho(t) = \frac{N(t)}{A} \quad (5)$$

729 In which, N is the total number of events, and A is the area of the map (e.g.
730 the number of grid points). By definition, $\varrho(t) \leq 1$ ($\varrho(t) = 1$ implies events are
731 occurring at every single grid point). The average number of near neighbours is a
732 function of distance (or area which is proportional to the distance squared), and
733 is given as:

$$V(r, t) = \frac{1}{N} \sum_{i=1}^N \sum_{j=1}^N (-\delta_{ij} - 1) I(d_{ij} \leq r, t) \quad (6)$$

734 Index i represents the summation over all existing events, and index j repre-
735 sents the other events. d_{ij} is the distance between them:

$$d_{ij} = |\mathbf{x}_i - \mathbf{x}_j| \quad (7)$$

736 We have used the Kronecker delta function:

$$\delta_{ij} = \begin{cases} 1, & \text{if } i = j \\ 0, & \text{if } i \neq j \end{cases} \quad (8)$$

737 Therefore, $-(\delta_{ij} - 1)$ denotes the self-exclusion during near neighbour count-
738 ing. If there is spatial clustering of events, the number of near neighbours ($V(r, t)$)
739 to any existing event is higher than the value expected by computing the average
740 background density:

$$V(r, t) > \varrho(t)\pi r^2 - 1 \quad (9)$$

741 The Ripley K-function is defined as the number of near neighbours divided by
742 the average density:

$$K(r, t) = \frac{V(r, t)}{\varrho(t)} \quad (10)$$

743 The Ripley K-function has the dimensions of area (radius squared), and is the
744 non-clustered area (grid boxes) needed to match the number of events as observed
745 in a localized clustered area. By definition, it is not defined if there is only one event
746 (i.e. there are 0 near neighbours). If spatial density is perfectly uniform, then the
747 Ripley K-function is exactly the geometric area of a circle with radius r . If events
748 occur as Poisson processes in space (i.e. each events occurring independently with
749 each other), the Ripley K-function is approximately but not exactly the same circle
750 geometric area. If events are clustered, then the Ripley K-function at a given radius
751 exceeds the geometric area of the circle given with the same radius:

$$K(r, t) \begin{cases} \approx \pi r^2, & \text{if events are not clustered} \\ > \pi r^2, & \text{if events are clustered} \end{cases} \quad (11)$$

752 Simulation study by Ripley (1979) show that the spatial Poisson process null
 753 hypothesis can be rejected at the 0.05 and 0.01 level if the observed supermum
 754 (maximum) Besag L-function exceeds a total area (A) dependent threshold:

$$\sup_r(L(r)) \geq 1.42 \frac{\sqrt{A}}{N}, p = 0.05 \quad (12)$$

$$\sup_r(L(r)) \geq 1.68 \frac{\sqrt{A}}{N}, p = 0.01 \quad (13)$$

755 In the present analysis, all individual K-functions that the null hypothesis
 756 cannot be rejected at the 0.05 level are excluded from the time average.

757 The above assumes that event sampling is not limited by domain specifications.
 758 In our datasets, we have undefined points because of:

- 759 – No observations outside of model/observation domain;
- 760 – Observations over water are undefined, and model non-land points are masked
 761 out.

762 This leads to under-sampling as there are unobserved events over the undefined
 763 area. Therefore, a correction factor (w) (Ripley, 1977) should be used on $V(r)$. We
 764 denote the corrected $V(r)$ with a “hat”.

$$\hat{V}(r, t) = \frac{1}{N} \sum_{i=1}^N \sum_{j=1}^N w |\delta_{ij} - 1| I(d_{ij} \leq r, t) \quad (14)$$

$$\hat{K}(r, t) = \frac{\hat{V}(r, t)}{\varrho(t)} \quad (15)$$

765 We have used an area based correction by Besag (1977) (discussed in the
 766 postscript of the original Ripley paper) due to its easy implementation with com-
 767 plex coastlines (problem degenerates to counting undefined grid boxes). Given a
 768 circle with radius r with only an area \hat{A} within the defined domain (over land and
 769 within the SUK domain), the correction factor is defined as:

$$w(r, x_0, y_0) = \frac{\pi r^2}{\hat{A}(r, x_0, y_0)} \quad (16)$$

770 Functions V and K are generally time dependent (maps of daily precipitation).
 771 We compute daily ϱ , V , and K values, and present only their time-averaged values.

$$\langle \hat{\varrho} \rangle = \frac{1}{T} \sum_{t=1}^T \varrho(t) \quad (17)$$

772

$$\langle \hat{V} \rangle(r) = \frac{1}{T} \sum_{t=1}^T \hat{V}(r, t) \quad (18)$$

773

$$\langle \hat{K} \rangle(r) = \frac{1}{T} \sum_{t=1}^T \hat{K}(r, t) \quad (19)$$

774 If events are not clustered, $K(A)$ is a linear function ($K(A = \pi r^2) \approx \rho A$).
 775 Since the area (A) is known for any given radius (r), K-function is often plotted
 776 as a square root (the Besag L-function) (Besag, 1977).

$$L(r) = \sqrt{\frac{K(r)}{\pi}} - r \quad (20)$$

777 Clustering is largest where $L(r)$ is largest, and unclustered data will have
 778 $L(r) \approx 0$. Note that both the K- and L-function are normalized in a way that
 779 they do not favour higher average spatial density. Both functions only measure *the*
 780 *inflation of local density due to event clustering*.

781 Since zonal (δx) and meridional (δy) grid point distances can only take on
 782 whole number values (0, 1, 2, 3, ...; “quantized grid space”), and can be diagonal.
 783 r is defined as:

$$r(\delta x, \delta y) = \sqrt{\delta x^2 + \delta y^2} \quad (21)$$

784 Note that $L(r)$ and $K(r)$ are functions of r . We have assumed the clustering and
 785 density to be isotropic (independent of direction), which is not true in general for
 786 precipitation (such as frontal and orographic precipitation). The sampled region
 787 is also assumed to be uniform. That is the same as saying the mechanisms behind
 788 rainfall within each region is assumed to be the same everywhere. We mimic that
 789 by sampling only the north-western orographic or south-eastern convective rain
 790 regions. That is, of course, only an approximation; non-uniformity clearly exists
 791 within each of the regions - such as non-uniform topography, changing land surface
 792 types, and irregular coastlines. A perfect stationary region is impossible to obtain,
 793 and we approximate that by slicing our domain with the Tees-Exe Line.

794 **List of Figures**

795	1	The Europe/North African (left) and southern UK (SUK) (right)	
796		domain. The inner domain is marked as a square on the left panel.	
797		Surface height (m, in the 12-km simulation) for the SUK domain	
798		is contoured with a 100-metre interval. For SUK, the north west	
799		(south east) sub-domain is coloured in light (dark) blue. There are	
800		a total of 464 (638) grid points in the north-west (south-east) sub-	
801		domain.	23
802	2	Observed 1991-2007 climatological daily precipitation (mm/day) at	
803		the 50-km scale (panels a-d) for different 3-month periods: March-	
804		April-May (MAM), June-July-August (JJA), September-October-	
805		November (SON), and December-January-February (DJF). The 50-	
806		km and 12-km (upscaled to 50-km) simulation's fractional departure	
807		from the observed values are shown in panels e to l. Only differences	
808		that are significant at the 5% level and larger than ± 0.1 are shown.	24
809	3	Same as in Fig. 2, but at the 12-km scale and the comparisons are	
810		made against the 12-km and 1.5-km simulations.	25
811	4	Average frequencies (days/year) that daily precipitation surpasses	
812		the 20 mm/day threshold during JJA+SON (upper half, a-f) and	
813		DJF+MAM (lower half, g-l) between 1991 and 2007 at each grid	
814		point. Panels a-c (JJA+SON) and g-i (DJF+MAM) show the fre-	
815		quencies for observations, 50-km and 12-km simulations at the 50-	
816		km scale with observations and 12-km daily amounts pre-upscaled	
817		to 50-km scale. Panels d-f (JJA+SON) and j-l (DJF+MAM) show	
818		the same at the 12-km scale for observations, 12-km and 1.5-km	
819		simulations.	26
820	5	Same as Fig. 4, but with a 50mm/day threshold.	27
821	6	The fractional differences in average intensity relative to observa-	
822		tions ($\frac{\langle P'_{\text{MODEL}} \rangle}{\langle P'_{\text{OBS}} \rangle}$, upper panels) and average event counts per year	
823		($\frac{N_{\text{MODEL}}}{\text{Number of years}}$ and $\frac{N_{\text{OBS}}}{\text{Number of years}}$, lower panels) for precipitation	
824		exceeding a range of thresholds, for all JJAs between 1991 and 2007.	
825		For the upper panels, filled symbol indicates the fractional differ-	
826		ences are significant at the 10% level. No symbols are drawn if there	
827		are zero samples from either the model or observations (see lower	
828		panels c and d). For average event counts, y-axis is plotted with a	
829		logarithmic scale.	28
830	7	Same as in Fig. 6, but for all DJFs between 1991 and 2007.	29

831	8	Shown above is a schematic of (a) non-clustered and (b) clustered precipitation. The spatial density of (a) is the same as (b); there are thirty precipitating grid points (dark spots) enclosed within the same area. For (a) the non-clustered case, individual grid point “showers” are approximately spaced at regular spatial intervals. For (b) the clustered case, precipitation organize into clustered “blobs” (light grey circles). One would expect (gridded) precipitation to cluster in space across a of spatial scales. If horizontal resolution is small enough ($\approx 1\text{km}$, clustering can be caused by convective clouds occupying more than one grid point. Precipitation and clouds are also clustered in the meso- (fronts, organized convective storms, orographic precipitation), synoptic- (mid-latitude and tropical low pressure systems), and planetary scales (ITCZ, monsoon systems).	30
832			
833			
834			
835			
836			
837			
838			
839			
840			
841			
842			
843			
844	9	The time average of three spatial descriptive statistic for JJA days with at least 2 grid points that has exceeded the 20mm/day threshold are shown. Days with clustering that cannot be rejected at the 5% level with the Poisson process null hypothesis are excluded. In the left panels (a and c), solid lines are the observed number of events (plus itself) from an existing event, and the dashed lines are the expected number of events (plus itself) if spatial density is uniform in space. In the right panels (b and d), the Besag L-function (local increase of spatial density due to spatial clustering) are plotted. Black, red, and green represent gridded observations, 12-km RCM, and 1.5-km RCM estimates respectively. The upper panels (a and b) are for the NW, and the lower panels (c and d) are for the SE.	31
845			
846			
847			
848			
849			
850			
851			
852			
853			
854			
855			
856			
857	10	Same as in Fig. 9, but the threshold is set to 50 mm/day.	32
858	11	Same as in Fig. 9 with the 20mm/day threshold, but for DJF instead of JJA.	33
859			
860	12	Similar as in Fig. 10 with the 50mm/day threshold, but for DJF instead of JJA. For SE, only 1.5-km model simulated values are shown; there are only 1 and 3 DJF SE 50mm/day valid events (events that have more than 1 grid point) in the observations and the 12-km model simulations respectively. The 1.5-km simulation has 12 SE events.	34
861			
862			
863			
864			
865			

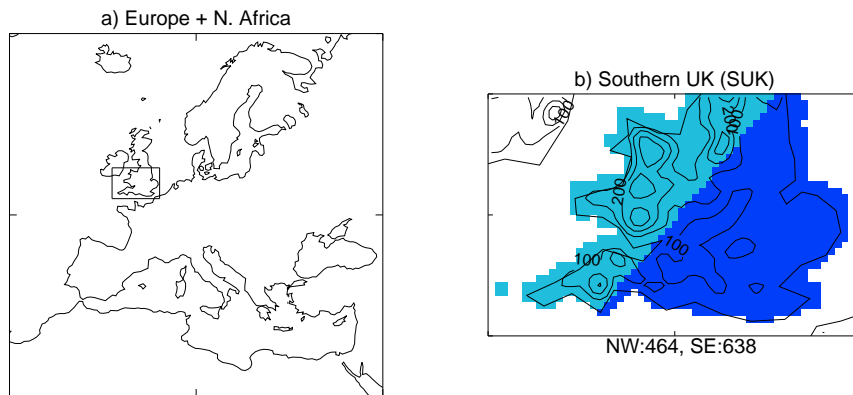


Fig. 1: The Europe/North African (left) and southern UK (SUK) (right) domain. The inner domain is marked as a square on the left panel. Surface height (m, in the 12-km simulation) for the SUK domain is contoured with a 100-metre interval. For SUK, the north west (south east) sub-domain is coloured in light (dark) blue. There are a total of 464 (638) grid points in the north-west (south-east) sub-domain.

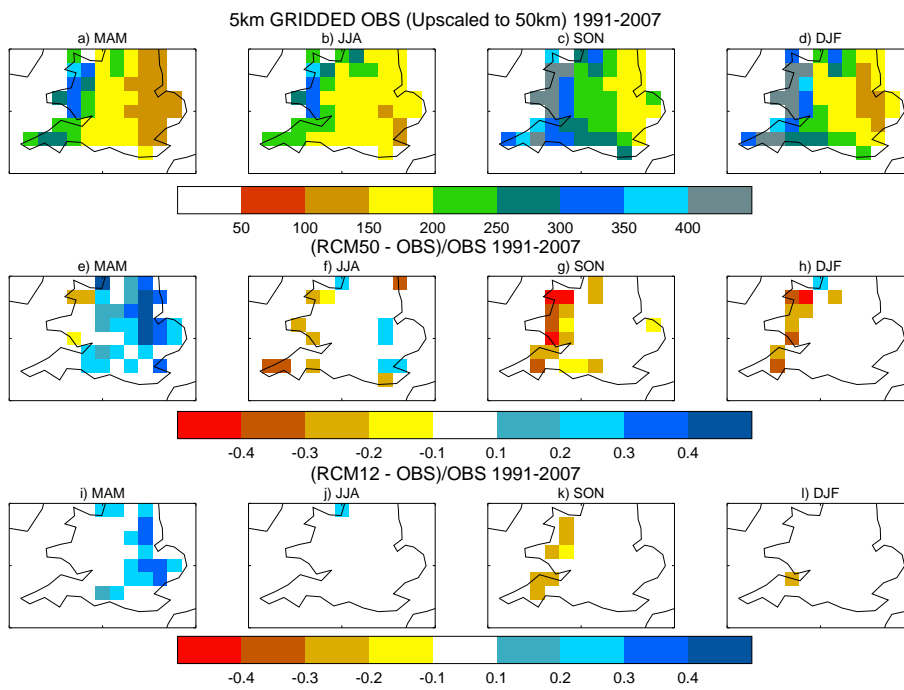


Fig. 2: Observed 1991-2007 climatological daily precipitation (mm/day) at the 50-km scale (panels a-d) for different 3-month periods: March-April-May (MAM), June-July-August (JJA), September-October-November (SON), and December-January-February (DJF). The 50-km and 12-km (upscaled to 50-km) simulation's fractional departure from the observed values are shown in panels e to l. Only differences that are significant at the 5% level and larger than ± 0.1 are shown.

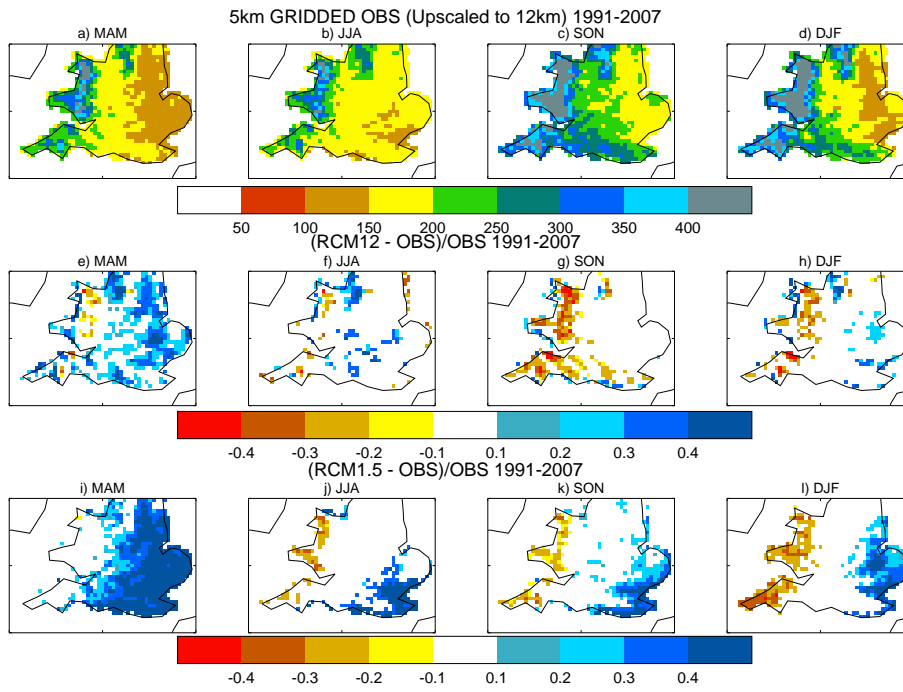


Fig. 3: Same as in Fig. 2, but at the 12-km scale and the comparisons are made against the 12-km and 1.5-km simulations.

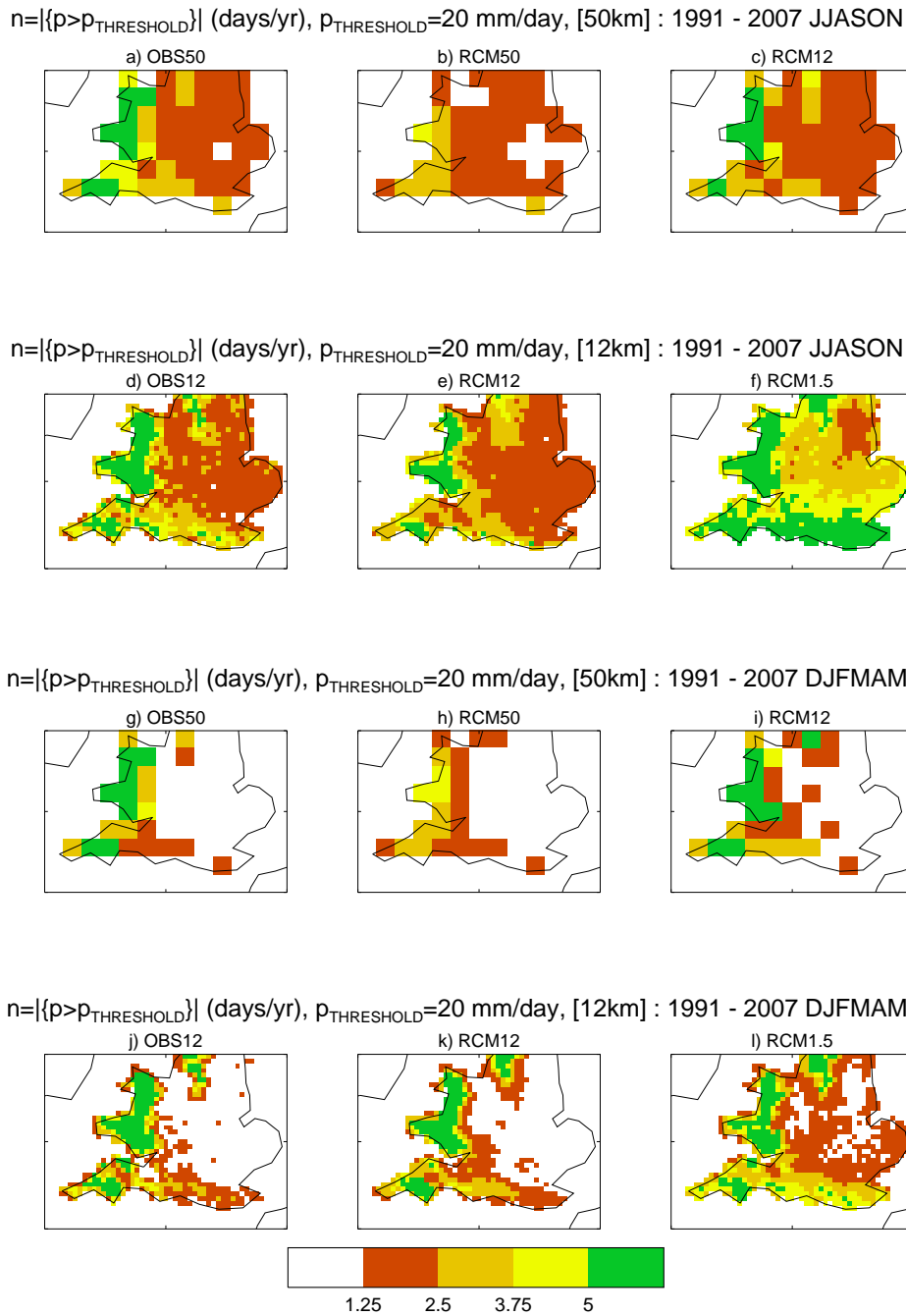
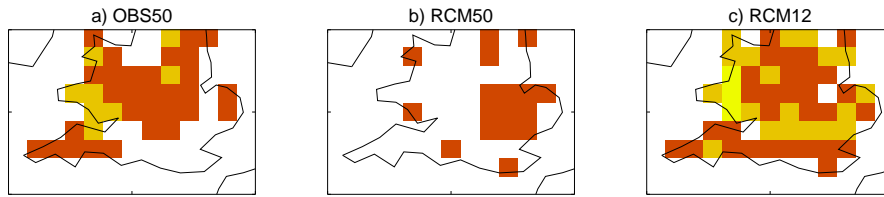
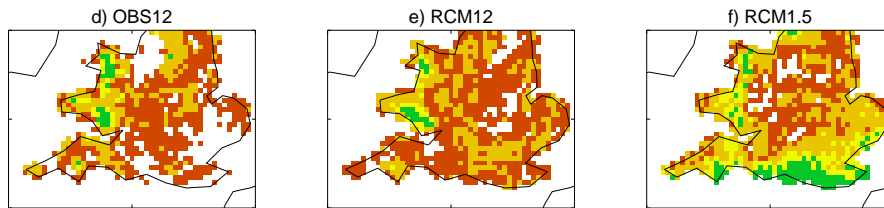


Fig. 4: Average frequencies (days/year) that daily precipitation surpasses the 20 mm/day threshold during JJA+SON (upper half, a-f) and DJF+MAM (lower half, g-l) between 1991 and 2007 at each grid point. Panels a-c (JJA+SON) and g-i (DJF+MAM) show the frequencies for observations, 50-km and 12-km simulations at the 50-km scale with observations and 12-km daily amounts pre-upscaled to 50-km scale. Panels d-f (JJA+SON) and j-l (DJF+MAM) show the same at the 12-km scale for observations, 12-km and 1.5-km simulations.

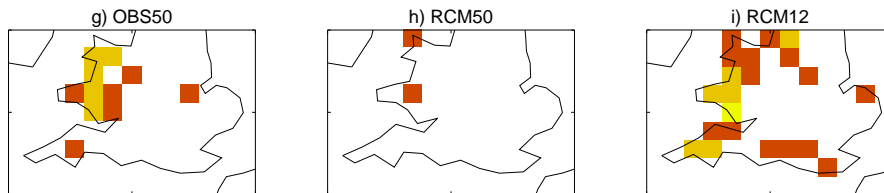
$n = |\{p > p_{\text{THRESHOLD}}\}|$ (days/yr), $p_{\text{THRESHOLD}} = 50$ mm/day, [50km] : 1991 - 2007 JJASON



$n = |\{p > p_{\text{THRESHOLD}}\}|$ (days/yr), $p_{\text{THRESHOLD}} = 50$ mm/day, [12km] : 1991 - 2007 JJASON



$n = |\{p > p_{\text{THRESHOLD}}\}|$ (days/yr), $p_{\text{THRESHOLD}} = 50$ mm/day, [50km] : 1991 - 2007 DJFMAM



$n = |\{p > p_{\text{THRESHOLD}}\}|$ (days/yr), $p_{\text{THRESHOLD}} = 50$ mm/day, [12km] : 1991 - 2007 DJFMAM

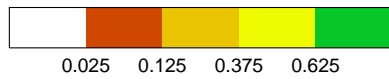
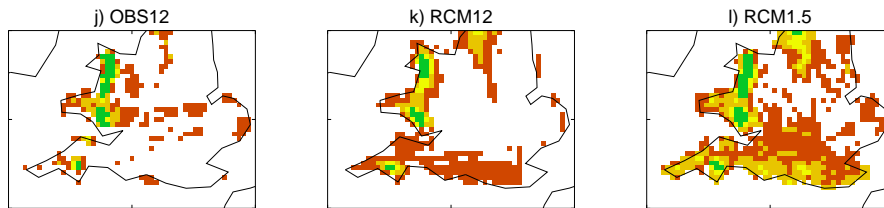


Fig. 5: Same as Fig. 4, but with a 50mm/day threshold.

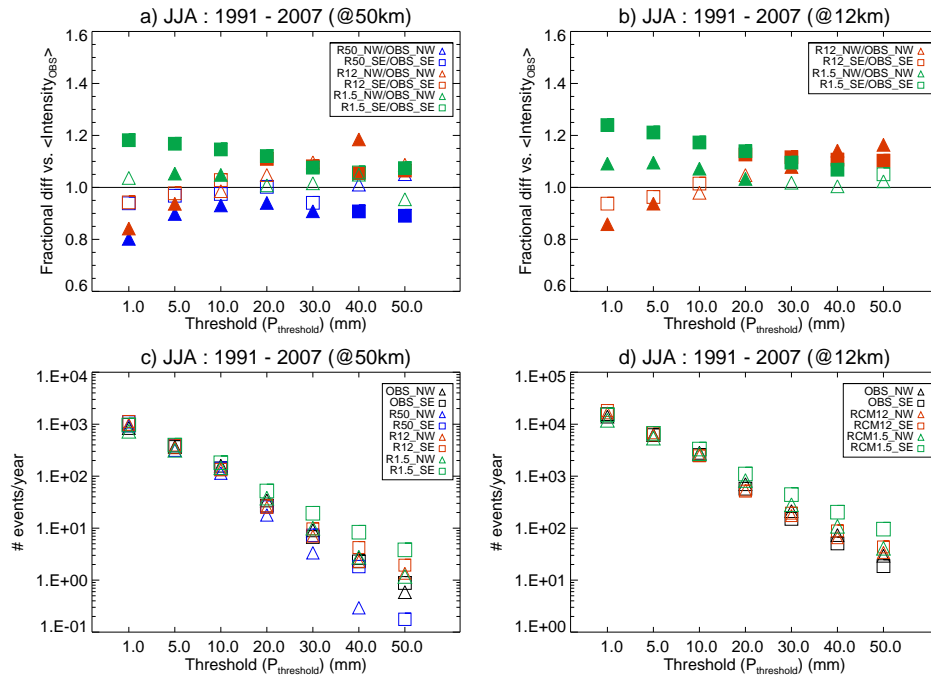


Fig. 6: The fractional differences in average intensity relative to observations ($\frac{\langle P_{\text{MODEL}} \rangle}{\langle P_{\text{OBS}} \rangle}$, upper panels) and average event counts per year ($\frac{N_{\text{MODEL}}}{\text{Number of years}}$ and $\frac{N_{\text{OBS}}}{\text{Number of years}}$, lower panels) for precipitation exceeding a range of thresholds, for all JJAs between 1991 and 2007. For the upper panels, filled symbol indicates the fractional differences are significant at the 10% level. No symbols are drawn if there are zero samples from either the model or observations (see lower panels c and d). For average event counts, y-axis is plotted with a logarithmic scale.

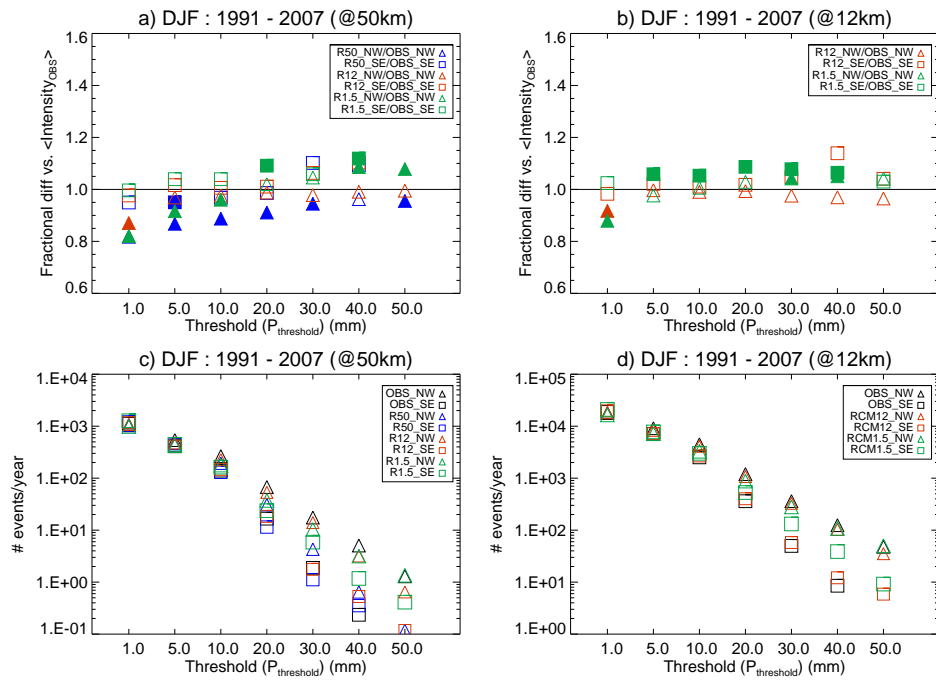


Fig. 7: Same as in Fig. 6, but for all DJFs between 1991 and 2007.

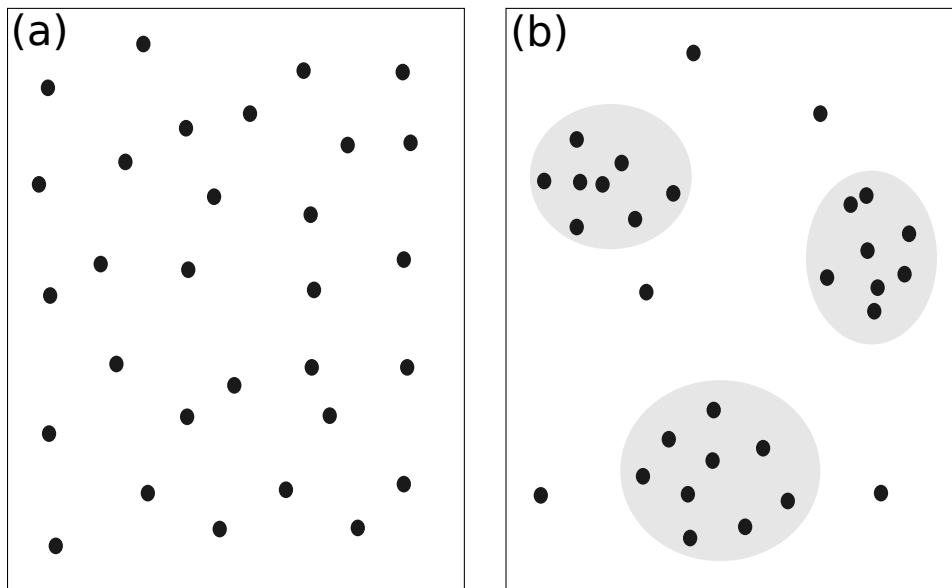


Fig. 8: Shown above is a schematic of (a) non-clustered and (b) clustered precipitation. The spatial density of (a) is the same as (b); there are thirty precipitating grid points (dark spots) enclosed within the same area. For (a) the non-clustered case, individual grid point “showers” are approximately spaced at regular spatial intervals. For (b) the clustered case, precipitation organize into clustered “blobs” (light grey circles). One would expect (gridded) precipitation to cluster in space across a of spatial scales. If horizontal resolution is small enough ($\approx 1\text{km}$, clustering can be caused by convective clouds occupying more than one grid point. Precipitation and clouds are also clustered in the meso- (fronts, organized convective storms, orographic precipitation), synoptic- (mid-latitude and tropical low pressure systems), and planetary scales (ITCZ, monsoon systems).

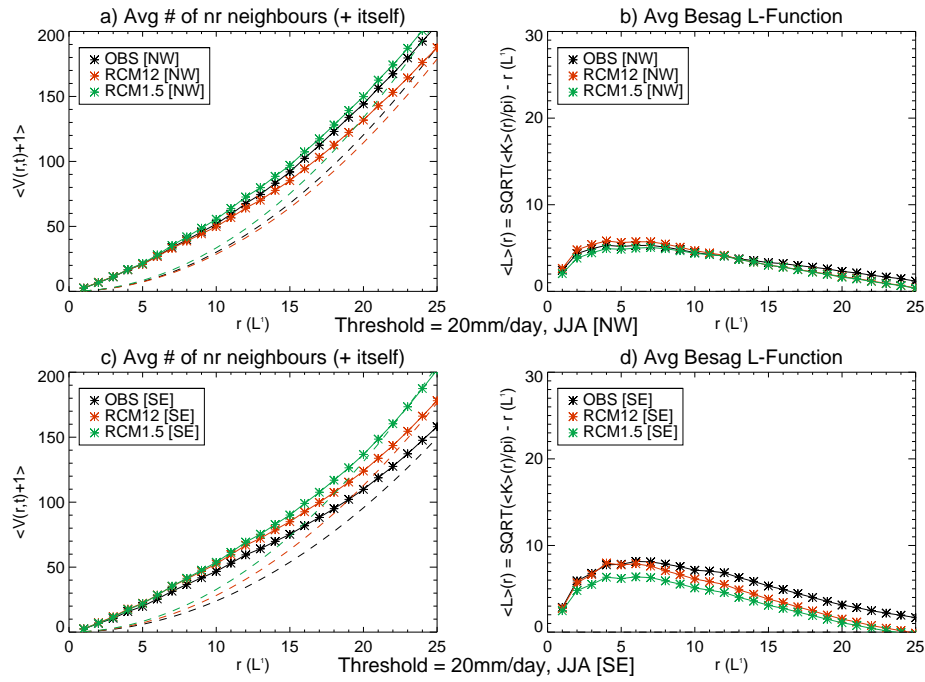


Fig. 9: The time average of three spatial descriptive statistic for JJA days with at least 2 grid points that has exceeded the 20mm/day threshold are shown. Days with clustering that cannot be rejected at the 5% level with the Poisson process null hypothesis are excluded. In the left panels (a and c), solid lines are the observed number of events (plus itself) from an existing event, and the dashed lines are the expected number of events (plus itself) if spatial density is uniform in space. In the right panels (b and d), the Besag L-function (local increase of spatial density due to spatial clustering) are plotted. Black, red, and green represent gridded observations, 12-km RCM, and 1.5-km RCM estimates respectively. The upper panels (a and b) are for the NW, and the lower panels (c and d) are for the SE.

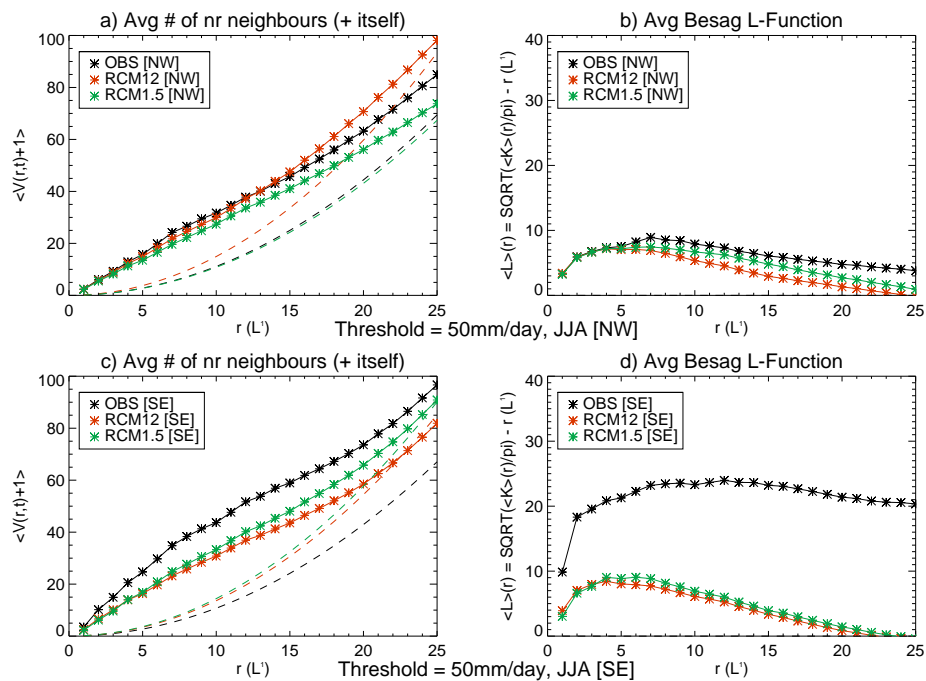


Fig. 10: Same as in Fig. 9, but the threshold is set to 50 mm/day.

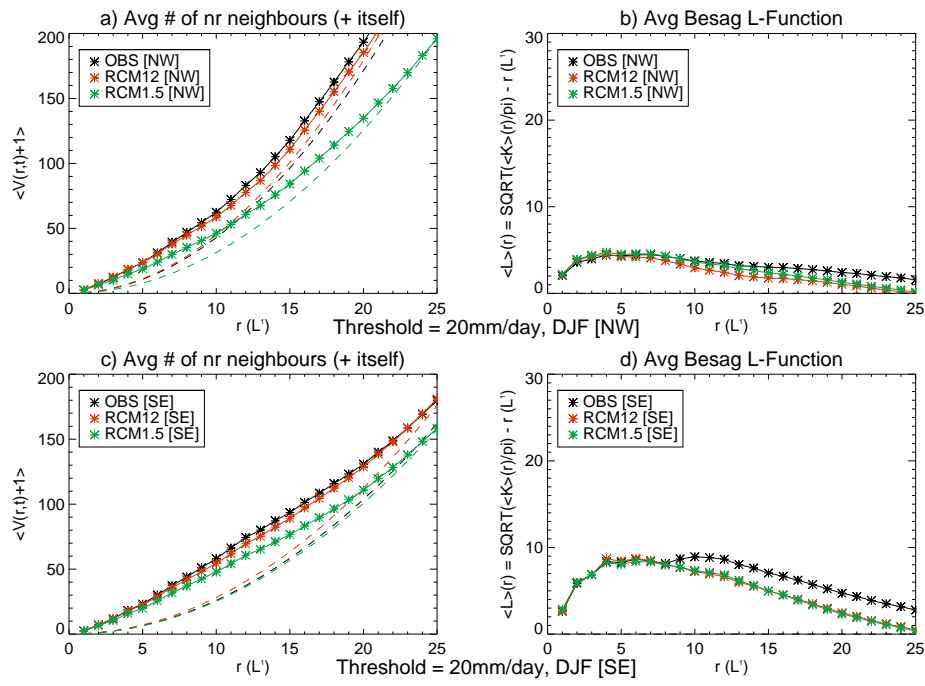


Fig. 11: Same as in Fig. 9 with the 20mm/day threshold, but for DJF instead of JJA.

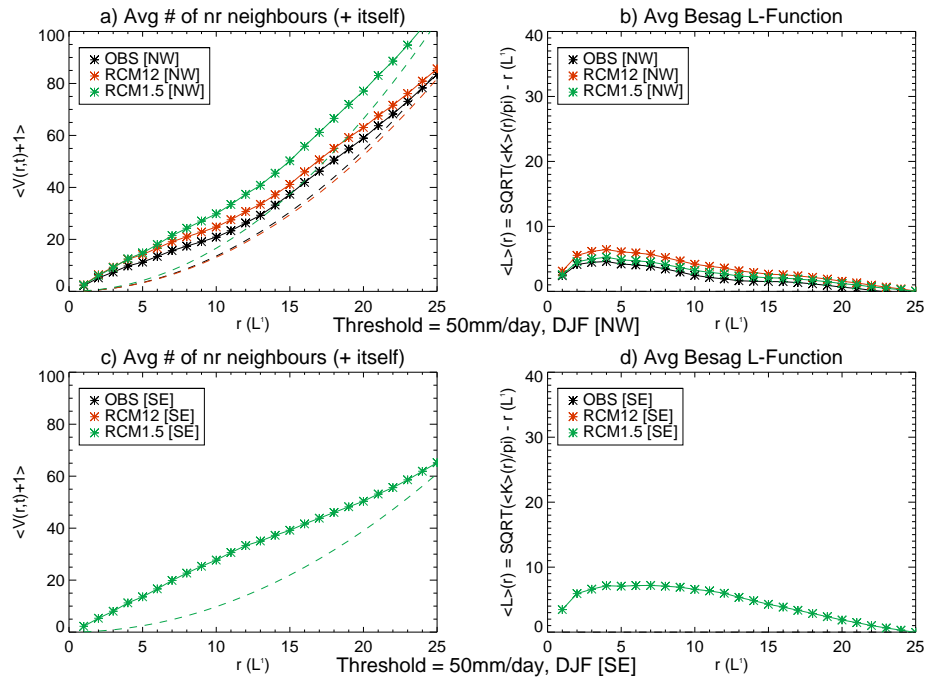


Fig. 12: Similar as in Fig. 10 with the 50mm/day threshold, but for DJF instead of JJA. For SE, only 1.5-km model simulated values are shown; there are only 1 and 3 DJF SE 50mm/day valid events (events that have more than 1 grid point) in the observations and the 12-km model simulations respectively. The 1.5-km simulation has 12 SE events.

866 **List of Tables**

867	1	Description of model simulations: RCM horizontal resolution (δx),	
868		model used, time-step (δt), number of vertical levels (N_z), simula-	
869		tion domain, lateral boundary conditions, convective parametrisation	36
870	2	The number of JJA and DJF days (out of the total number of	
871		valid JJA and DJF days) where there is at least one daily-threshold	
872		excess event anywhere in domain at the 12-km scale	36
873	3	Average 20 + <i>mm/day</i> and 50 + <i>mm/day</i> event density (events per	
874		grid box) for JJA and DJF for the NW	36
875	4	Average 20 + <i>mm/day</i> and 50 + <i>mm/day</i> event density (events per	
876		grid box) for JJA and DJF for the SE	36

Table 1: Description of model simulations: RCM horizontal resolution (δx), model used, time-step (δt), number of vertical levels (N_z), simulation domain, lateral boundary conditions, convective parametrisation

δx	Model	$\delta t, N_z$	Domain	LBC	CP
50km	HadGEM3-RA	720sec, 63	Eur.+N. Africa	ERA-Int.	CMODS
12km	HadGEM3-RA	300sec, 63	Eur.+N. Africa	ERA-Int.	CMODS
1.5km	modified UKV	50sec, 70	SUK	12-km RCM	No CP

Table 2: The number of JJA and DJF days (out of the total number of valid JJA and DJF days) where there is at least one daily-threshold excess event anywhere in domain at the 12-km scale

— Threshold	(a) Obs. (12-km)	(b) 12-km RCM	(c) 1.5-km RCM
20+ mm/day (JJA)	544 / 1564	405 / 1564	564 / 1564
30+ mm/day (JJA)	314 / 1564	215 / 1564	359 / 1564
40+ mm/day (JJA)	163 / 1564	148 / 1564	233 / 1564
50+ mm/day (JJA)	75 / 1564	97 / 1564	149 / 1564
20+ mm/day (DJF)	528 / 1534	429 / 1534	540 / 1534
30+ mm/day (DJF)	304 / 1534	218 / 1534	303 / 1534
40+ mm/day (DJF)	166 / 1534	98 / 1534	157 / 1534
50+ mm/day (DJF)	88 / 1534	56 / 1534	79 / 1534

Table 3: Average 20+ mm/day and 50+ mm/day event density (events per grid box) for JJA and DJF for the NW

— Season Threshold	(a) JJA 20+ mm/day	(b) JJA 50+ mm/day	(c) DJF 20+ mm/day	(d) DJF 50+ mm/day
OBS	0.096	0.035	0.136	0.043
12-km RCM	0.091	0.047	0.143	0.042
1.5-km RCM	0.106	0.034	0.100	0.053

Table 4: Average 20+ mm/day and 50+ mm/day event density (events per grid box) for JJA and DJF for the SE

— Season Threshold	(a) JJA 20+ mm/day	(b) JJA 50+ mm/day	(c) DJF 20+ mm/day	(d) DJF 50+ mm/day
OBS	0.076	0.034	0.083	—
12-km RCM	0.090	0.043	0.090	—
1.5-km RCM	0.104	0.046	0.080	0.031

877 **Acknowledgements** This research is part of the CONVEX project - a collaboration between
878 Newcastle University, the Met Office, and the University of Exeter. CONVEX is supported by
879 the United Kingdom NERC Changing Water Cycle programme (grant NE/I006680/1), and the
880 presented model simulations are supported by the Met Office. The lead author is financially
881 supported by Newcastle University, and is a visiting scientist at the Met Office Hadley Centre
882 in Exeter, United Kingdom.

883 **References**

- 884 Allan RP, Soden BJ, John VO, Ingram W, Good P (2010) Current changes in
885 tropical precipitation. *Environ Res Lett* 5(2):025,205, DOI 10.1088/1748-9326/
886 5/2/025205
- 887 Allen MR, Ingram WJ (2002) Constraints on future changes in climate and the
888 hydrologic cycle. *Nature* 419:224–232
- 889 Antic S, Laprise R, Denis B, de Elía R (2006) Testing the downscaling ability of a
890 one-way nested regional climate model in regions of complex topography. *Clim*
891 *Dyn* 26(2-3):305–325, DOI 10.1007/s00382-005-0046-z
- 892 Arakawa A (2004) The cumulus parameterization problem: Past, present, and
893 future. *J Climate* 17(13):2493–2525, DOI 10.1175/1520-0442(2004)017<2493:
894 RATCPP>2.0.CO;2
- 895 Arakawa A, Lamb VR (1977) Computational design of the basic dynamical pro-
896 cesses of the UCLA general circulation model. *Methods Comput Phys* 17:173–
897 265
- 898 Besag JE (1977) Comments on ripley’s paper. *J Roy Stat Soc* 39(2):193–195
- 899 Blackburn M, Methven J, Roberts N (2008) Large-scale context for the uk floods
900 in summer 2007. *Weather* 63(9):280–288, DOI 10.1002/wea.322
- 901 Charney JG, Phillips NA (1953) Numerical integration of the quasi-geostrophic
902 equations for barotropic and simple baroclinic flows. *J Meteorol* 10:71–99, DOI
903 10.1175/1520-0469(1953)010<0071:NIOTQG>2.0.CO;2
- 904 Davies T, Cullen MJP, Malcolm AJ, Mawson MH, Stainforth A, White AA,
905 Wood N (2005) A new dynamical core for the Met Office’s global and regional
906 modelling of the atmosphere. *Q J R Meteorol Soc* 131(608):1759–1782, DOI
907 10.1256/qj.04.101
- 908 Dee DP, Uppala SM, Simmons AJ, Berrisford P, Poli P, Kobayashi S, Andrae U,
909 Balmaseda MA, Balsamo G, Bauer P, Bechtold P, Beljaars ACM, van de Berg L,
910 Bidlot J, Bormann N, Delsol C, Dragani R, Fuentes M, Geer AJ, Haimberger L,
911 Healy SB, Hersbach H, Hölm EV, Isaksen L, Kallberg P, Köhler M, Matricardi
912 M, McNally AP, Monge-Sanz BM, Morcrette JJ, Park PK, Peubey C, de Ros-
913 nay P, Tavolato C, Thépaut JN, Vitart F (2011) The ERA-Interim reanalysis:
914 configuration and performance of the data assimilation system. *Q J R Meteorol*
915 *Soc* 137(656):553–597, DOI 10.1002/qj.828
- 916 Déqué M, Piedelievre JP (1995) High resolution climate simulation over Europe.
917 *Clim Dyn* 11:321–339
- 918 Efron B, Tibshirani RJ (1993) *An Introduction to the Bootstrap*, Monographs on
919 *Statistics and Applied Probability*, vol 57. Chapman and Hall, New York
- 920 Ensor LA, Robeson SM (2008) Statistical characteristics of daily precipitation:
921 Comparisons of gridded and point datasets. *J Appl Meteorol Clim* 47:2468–
922 2476, DOI 10.1175/2008JAMC1757.1
- 923 Essery R, Best M, Cox P (2001) MOSES 2.2 technical documentation. Hadley
924 Centre Technical Note 30, Hadley Centre, Met Office, Fitzroy Road, Exeter,
925 UK
- 926 Faulkner D (1999) *Flood estimation handbook*. Volume 2. Rainfall frequency es-
927 timation. NERC Centre for Ecology and Hydrology
- 928 Fowler HJ, Ekström M (2009) Multi-model ensemble estimates of climate change
929 impacts on UK seasonal precipitation extremes. *Int J Climatol* 29:385–416

- 930 Fowler HJ, Ekstrom M, Blenkinsop S, Smith AP (2007) Estimating change in
931 extreme European precipitation using a multi-model ensemble. *J Geophys Res*
932 112(D18), art No. D18104
- 933 Giorgi F, Marinucci MR (1996) An investigation of the sensitivity of simulated
934 precipitation to the model resolution and its implication for climate studies. *Mon*
935 *Weather Rev* 124:148–166, DOI 10.1175/1520-0493(1996)124<0148:AIOTSO>2.
936 0.CO;2
- 937 Golding BW (1998) Nimrod: A system for generating automated very short range
938 forecasts. *Meteorol Appl* 5:1–16
- 939 Gregory D, Rowntree PR (1990) A mass-flux convection scheme with rep-
940 resentation of cloud ensemble characteristics and stability dependent clo-
941 sure. *Mon Weather Rev* 118:1483–1506, DOI 10.1175/1520-0493(1990)118<1483:
942 AMFCSW>2.0.CO;2
- 943 Hohengegger C, Brockhaus P, Schär C (2008) Towards climate simulations at cloud-
944 resolving scales. *Meteorol Z* 17(4):383–394, DOI 10.1127/0941-2948/2008/0303
- 945 Hong SY, Leetmaa A (1999) An evaluation of the ncep rsm for regional climate
946 modeling. *J Climate* 12(2):592–609, DOI 10.1175/1520-0442(1999)012<0592:
947 AEOTNR>2.0.CO;2
- 948 Jones RG, Murphy JM, Noguer M (1995) Simulation of climate change over Europe
949 using a nested regional–climate model. I: Assessment of control climate, includ-
950 ing sensitivity to location of lateral boundaries. *Q J R Meteorol Soc* 121:1413–
951 1449
- 952 Jones RG, Murphy JM, Noguer M, Keen AB (1997) Simulation of climate change
953 over Europe using a nested regional–climate model. II: Comparison of driving
954 and regional model responses to a doubling of carbon dioxide concentration. *Q*
955 *J R Meteorol Soc* 123:265–292
- 956 Kendon EJ, Roberts NM, Senior CA, Roberts MJ (in press) Realism of rain-
957 fall in a very high resolution regional climate model. *J Climate* DOI 10.1175/
958 JCLI-D-11-00562.1
- 959 Knot C, Heinemann G, Rockel B (2010) Changes in weather extremes: Assessment
960 of return values using high resolution climate simulations at convection-resolving
961 scale. *Meteorol Z* 19(1):11–23, DOI 10.1127/0941-2948/2010/0424
- 962 Laprise R, de Elía R, Caya D, Biner S, Lucas-Picher P, Diaconescu E,
963 Leduc M, Alexandru A, Separovic L (2008) Challenging some tenets of re-
964 gional climate modelling. *Meteorol Atmos Phys* 100(1-4):3–22, DOI 10.1007/
965 s00703-008-0292-9
- 966 Lean HW, Clark PA, Dixon M, Roberts NM, Fitch A, Forbes R, Halliwell C (2008)
967 Characteristics of high-resolution versions of the Met Office Unified Model for
968 forecasting convection over the United Kingdom. *Mon Weather Rev* 136:3408–
969 3424, DOI 10.1175/2008MWR2332.1
- 970 Leduc M, Laprise R (2009) Regional climate model sensitivity to domain size.
971 *Clim Dyn* 32(6):833–854, DOI 10.1007/s00382-008-0400-z
- 972 Lilly DK (1962) On the numerical simulation of buoyant convection. *Tellus A*
973 14:148–171
- 974 Maraun D, Rust HW, Osborn TJ (2009) The annual cycle of heavy precipitation
975 across the united kingdom: a model based on extreme value statistics. *Int J*
976 *Climatol* 29(12):1731–1744, DOI 10.1002/joc.1811
- 977 Meehl GA, Karl T, Easterling DR, Changnon S, Changnon D, Jr RP, Evans J,
978 Groisman PY, Knutson TR, Kunkel KE, Mearns LO, Parmesan C, Pulwarty

- 979 R, Root T, Sylves RT, Whetton P, Zwiers F (2000) An introduction to trends
980 in extreme weather and climate events: Observations, socioeconomic impacts,
981 terrestrial ecological impacts, and model projections. *Bull Am Meteorol Soc*
982 81(3):413–416, DOI 1520-0477(2000)081<0413:AITTIE>2.3.CO;2
- 983 Molinari J, Dudek M (1992) Parameterization of convective precipitation in
984 mesoscale numerical models: A critical review. *Mon Weather Rev* 120(2):326–
985 344, DOI 10.1175/1520-0493(1992)120<0326:POCPIM>2.0.CO;2
- 986 Perry M, Hollis D, Elms M (2009) The Generation of Daily Gridded Datasets of
987 Temperature and Rainfall for the UK. Met Office National Climate Information
988 Centre, FitzRoy Road, Exeter, Devon EX1 3PB, United Kingdom
- 989 Rauscher SA, Coppola E, Piani C, Giorgi F (2010) Resolution effects on regional
990 climate model simulations of seasonal precipitation over Europe. *Clim Dyn*
991 35(4):685–711, DOI 10.1007/s00382-009-0607-7
- 992 Reynolds RW, Smith TM, Liu C, Chelton DB, Casey KS, Schlax MG (2007)
993 Daily high-resolution blended analyses for sea surface temperature. *J Climate*
994 20:5473–5496
- 995 Ripley BD (1977) Modelling spatial patterns. *J Roy Stat Soc* 39(2):172–212
- 996 Ripley BD (1979) Tests of ‘randomness’ for spatial point patterns. *J Roy Stat Soc*
997 41(3):368–374
- 998 Roberts NM, Lean HW (2008) Scale-selective verification of rainfall accumulations
999 from high-resolution forecasts of convective events. *Mon Weather Rev* 136:78–
1000 97, DOI 10.1175/2007MWR2123.1
- 1001 Roberts NM, Cole S, Forbes RM, Moore R, Boswell D (2009) Use of high-resolution
1002 NWP rainfall and river flow forecasts for advanced warning of the Carlisle flood,
1003 north-west England. *Meteorol Appl* 16(1):23–34, DOI 10.1002/met.94
- 1004 Seth A, Giorgi F (1998) The effects of domain choice on summer precipitation
1005 simulation and sensitivity in a regional climate model. *J Climate* 11:2698–2712,
1006 DOI 10.1175/1520-0442(1998)011<2698:TEODCO>2.0.CO;2
- 1007 Smagorinsky J (1963) General circulation experiments with the primitive equa-
1008 tions, Part 1: The basic experiments. *Mon Weather Rev* 91:99–164
- 1009 Wakazuki Y, Nakamura M, Kanada S, Muroi C (2008) Climatological reproducibil-
1010 ity evaluation and future climate projection of extreme precipitation events in
1011 the Baiu season using a high-resolution non-hydrostatic RCM in comparison
1012 with an AGCM. *J Meteorol Soc Jpn* 86(6):951–967
- 1013 Walters DN, Best MJ, Bushell AC, Copsey D, Edwards JM, Falloon PD, Harris
1014 CM, Lock AP, Manners JC, Morcrette CJ, Roberts MJ, Stratton RA, Webster S,
1015 Wilkinson JM, Willett MR, Boutle IA, Earnshaw PD, Hill PG, MacLachlan C,
1016 Martin GM, Moufouma-Okia W, Palmer MD, Petch JC, Rooney GG, Scaife AA,
1017 Williams KD (2011) The Met Office Unified Model global atmosphere 3.0/3.1
1018 and JULES global land 3.0/3.1 configurations. *Geosci Model Devel* 4:919–941,
1019 DOI 10.5194/gmd-4-919-2011
- 1020 Wigley TML, Lough JM, Jones PD (1984) Spatial patterns of precipitation in
1021 england and wales and a revised, homogeneous england and wales precipitation
1022 series. *Int J Climatol* 4(1):1–25, DOI 10.1002/joc.3370040102
- 1023 Wilks DS (1997) Resampling hypothesis tests for autocorrelated fields. *J Climate*
1024 10:65–82
- 1025 Wilson DR, Ballard SP (1999) A microphysically based precipitation scheme for
1026 the UK Meteorological Office Unified Model. *Q J R Meteorol Soc* 125:1607–1636

-
- 1027 Wilson DR, Bushell AC, Kerr-Munslow AM, Price JD, Morcrette CJ (2008) PC2:
1028 A prognostic cloud fraction and condensation scheme. I: Scheme description. Q
1029 J R Meteorol Soc 134:2093–2107, DOI 10.1002/qj.333